# 5. Experimental Results

## 5.1. The Ni-S system

### 5.1.1. Nickel – Ni-S melt assemblage (1100°C - 700°C)

#### 5.1.1.1. EPMA results

Major element compositions of co-existing nickel and Ni-S melt at 1100°C, 1000°C, 900°C and 700°C, as determined by EPMA, are given in Tables 8 to 11, with 3σ standard deviations. In addition to Ni and S, the total PGE content as determined by PIXE (Section 5.1.1.2.) is also given. The low calculated total for some metal phases (for example experiment HU441, Table 8, with a total of 98.21 wt%) does not take into account the PGE content, which, if considered, would bring the total elemental content close to 100 wt%.

EPMA determined Ni:S ratios were projected onto the Ni-S phase diagram (Figure 12 – blue triangles), ignoring the effect of PGE content, which is comparably very small. Average compositions of metals and melts were calculated with resampling statistics. The compositions can be compared to their expected compositions from the initial bulk compositions of the experimental charges. All the determined compositions of the melts were clearly more S-rich than predicted by the Ni-S phase diagram by Sharma and Chang (1980) and Cemic and Kleppa (1986).

***Table 8.*** *Major element compositions, determined by EPMA, of co-existing nickel and quenched melt equilibrated at 1100°C.*

| Exp | Phase | Ni wt% (± 3σ) | S wt% (± 3σ) | Total (wt%) | PGE# (wt%) | n |
|---|---|---|---|---|---|---|
| **HU437** | Nickel | 99.83 (0.35) | 0.04 (0.02) | 99.87 | ~0.1 | 40 |
| | Melt | 81.49 (1.02) | 18.53 (0.48) | 100.02 | ~0.1 | 34 |
| **HU441** | Nickel | 98.21 (0.34) | bd | 98.21 | ~1.8 | 22 |
| | Melt | 81.92 (1.03) | 18.37 (0.51) | 100.29 | ~0.4 | 24 |
| **HU731** | Nickel | 100.42 (0.43) | bd | 100.42 | ~0.4 | 32 |
| | Melt | 81.84 (0.96) | 18.03 (0.91) | 99.87 | ~0.1 | 26 |
| **HU733** | Nickel | 100.06 (0.59) | bd | 100.06 | ~0.3 | 26 |
| | Melt | 82.93 (1.28) | 17.66 (0.92) | 100.59 | ~0.2 | 26 |

# Estimation of total PGE content as determined by PIXE, discussed in section 5.1.1.2.

#### 5.1.1.1.1. Separated drops

A small drop separated from experiment HU441 (1100°C). EPMA analysis of the drop gave the Ni content at 78.84 wt% (1σ = 6.88 wt%), and the S content at 19.46 wt% (1σ = 6.19 wt%). Twenty spot analyses of 40 µm diameter were performed as the drop was too small to allow for area analyses, which accounts for the high standard deviations. PGE were below detection. The drop was also analysed separately during PIXE analyses, as discussed below. It is believed that the drop separated from the melt during quenching of the charge after equilibrium was established in the system, and has no influence on the results of the experiment.

A comparatively small drop found with experiment HU392 (1000°C) is shown in Figure 35. Investigation of the experimental charge revealed the absence of metal in the charge - despite three cross-sections cut through the charge none could be detected. The only detectable metal was found in the separated drop, which also contained melt. The drop separated from the bulk charge before equilibrium was reached, but equilibrium would have been achieved within this separated drop, considering its small size and an equilibration time of 35 days. The results of the melt analyses of experiment HU392, and the results of

the analyses on the separated drop, are shown in Table 9. The melt of the main charge was analysed in the same manner as the other melts in Table 9 (area analyses), but the separated drop was analysed with a 40 µm diameter spot (32 spot analyses), resulting in large standard deviations and uncertainty. Both the melt and metal in the separated drop were analysed for Rh, Pd and Pt. No PGE were detected in the melt, but in the metal 0.41 wt% Rh ($1\sigma$ = 0.12 wt %) and 2.31 wt% Pt ($1\sigma$ = 0.17 wt%) were. No Pd was detected in the metal. PIXE analyses were performed on all three phases (melt of the main experiment and metal and melt in the separated drop), and are discussed in the following section.

***Table 9.*** *Major element compositions, determined by EPMA, of co-existing nickel and quenched melt equilibrated at 1000°C.*

| Exp | Phase | Ni wt% (± 3σ) | S wt% (± 3σ) | Total (wt%) | PGE# (wt%) | n |
|---|---|---|---|---|---|---|
| **HU381** | Nickel | 97.46 (0.67) | bd | 97.46 | ~2.5 | 26 |
| | Melt | 80.56 (0.99) | 19.25 (1.08) | 99.81 | ~0.7 | 20 |
| **HU392** | Melt | 78.96 (0.49) | 20.04 (0.33) | 99.00 | - | 36 |
| **HU392** | Nickel | 96.54 (0.91) | bd | 96.54 | ~2.2 | 32 |
| **(drop)** | Melt | 77.27 (5.43) | 20.64 (5.93) | 97.91 | ~0.1 | 30 |
| **HU393** | Nickel | 99.57 (0.02) | bd | 99.57 | ~1.1 | 35 |
| | Melt | 80.92 (1.07) | 19.19 (0.90) | 100.11 | ~0.2 | 34 |
| **HU394** | Nickel | 92.95 (1.93) | bd | 92.95 | ~6.6 | 128 |
| | Melt | 80.04 (1.45) | 19.26 (1.16) | 99.30 | ~1.4 | 62 |
| **HU395** | Nickel | 88.05 (4.43) | bd | 88.05 | ~10.6 | 100 |
| | Melt | 79.33 (1.14) | 20.21 (0.86) | 99.54 | ~2.7 | 37 |
| **HU412** | Nickel | 89.44 (0.60) | bd | 89.44 | ~8.1 | 28 |
| | Melt | 79.36 (1.10) | 19.60 (0.95) | 98.96 | ~1.9 | 61 |

# Estimation of total PGE content as determined by PIXE, discussed in section 5.1.1.2.

***Table 10**. Major element compositions, determined by EPMA, of co-existing nickel and quenched melt equilibrated at 900°C.*

| Exp | Phase | Ni wt% (± 3σ) | S wt% (± 3σ) | Total (wt%) | PGE[#] (wt%) | n |
|---|---|---|---|---|---|---|
| **HU426** | Nickel | 98.43 (0.35) | bd | 98.43 | ~0.4 | 18 |
| | Melt | 79.20 (0.83) | 19.88 (0.78) | 99.08 | <0.1 | 53 |
| **HU427** | Nickel | 99.72 (0.95) | bd | 99.72 | ~0.3 | 16 |
| | Melt | 78.69 (1.05) | 21.14 (0.93) | 99.83 | ~0.3 | 35 |
| **HU428** | Nickel | 99.74 (0.45) | bd | 99.74 | ~0.6 | 34 |
| | Melt | 79.46 (0.73) | 20.93 (0.72) | 100.39 | ~0.1 | 42 |
| **HU429** | Nickel | 99.94 (0.62) | bd | 99.94 | ~1.6 | 18 |
| | Melt | 78.38 (0.66) | 21.36 (0.59) | 99.74 | ~0.4 | 30 |
| **HU753** | Nickel | 99.23 (1.03) | bd | 99.23 | ~0.8 | 46 |
| | Melt | 79.00 (0.73) | 21.66 (0.34) | 100.66 | ~0.2 | 30 |

# Estimation of total PGE content as determined by PIXE, discussed in section 5.1.1.2.

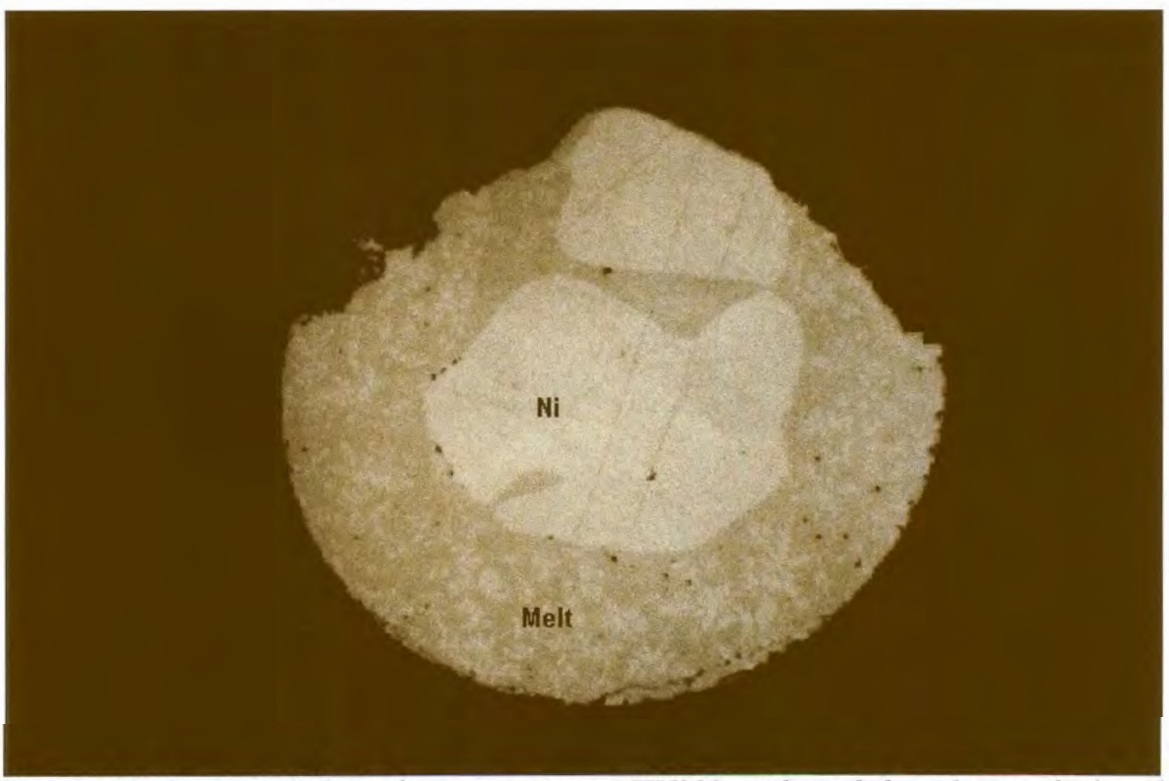


***Figure 35.** Separated drop from experiment HU392 with nickel and quenched melt equilibrated at 1000°C. Field of view 4 mm.*

***Table 11.*** *Major element compositions, determined by EPMA, of co-existing nickel and quenched melt, equilibrated at 700°C.*

| Exp | Phase | Ni wt% (± 3σ) | S wt% (± 3σ) | Total (wt%) | PGE# (wt%) | n |
|---|---|---|---|---|---|---|
| **HU469** | Nickel | 99.45 (0.49) | bd | 99.45 | ~0.3 | 30 |
| | Melt | 76.51 (0.65) | 22.34 (0.47) | 98.85 | ~0.1 | 54 |
| **HU471** | Nickel | 98.76 (0.40) | bd | 98.76 | ~1.1 | 30 |
| | Melt | 75.12 (1.98) | 23.95 (1.92) | 99.07 | <0.1 | 39 |
| **HU472** | Nickel | 99.48 (0.28) | bd | 99.48 | nd | 26 |
| | Melt | 76.95 (0.72) | 22.45 (0.19) | 99.40 | ~0.4 | 82 |
| **HU473** | Nickel | 99.43 (0.29) | bd | 99.43 | ~0.6 | 26 |
| | Melt | 77.60 (0.70) | 22.48 (0.58) | 100.08 | ~0.1 | 94 |

# Estimation of total PGE content as determined by PIXE, discussed in section 5.1.1.2.

A separated drop was also found with experiment HU395. This drop consisted only of melt, and was analysed for Ni, S, Rh, Pd and Pt with a 40 µm diameter beam spot (28 spot analyses). The melt contained 75.16 wt% Ni (1σ = 4.43 wt%), 22.52 wt% S (1σ = 5.16 wt%), no detectable Rh, 1.29 wt% Pd (1σ = 0.53 wt%), and no detectable Pt. The drop was also analysed by PIXE, as discussed below (Section 5.1.1.2.).

A very small separated drop found with experiment HU427 (900°C) consisted only of quenched melt, and was analysed for Ni, S, Rh, Pd and Pt with a beam spot of 40 µm diameter. From 10 analyses, 77.17 wt% Ni (1σ = 0.94 wt%), 21.70 wt% S (1σ = 0.45 wt%), and no PGE were detected. The drop probably separated from the charge during quenching, but was also analysed separately by PIXE, as discussed in the following section.

### 5.1.1.2. PIXE results

#### 5.1.1.2.1. Milli-PIXE

##### 5.1.1.2.1.1. Results for equilibration at 1100°C

Heterogeneity of the melt of experiment HU733 for the PGE, is indicated by the significant variation between the two analyses (Table 13), which could not be corrected for by the large diameter of the beam spot (~ 0.1 mm; see Photograph 36 for the heterogeneous texture). The Rh and Pd results of these two analyses were combined with resampling statistics (Table 20). As the Pt content from the second analysis is below detection, the value from the first analysis was used for further calculations (Table 20). Two analyses were performed on the melt phase of experiment HU731, where only Pt was added to the experiment. Considering the standard deviations, there is no significant difference between the two analyses. The two analyses were combined with resampling statistics for further calculations (Table 20).

***Table 12.*** *Milli-PIXE trace element spot analyses of nickel that co-exists with melt, equilibrated at 1100°C.*

| Exp | Rh wt% (± 3σ) | Rh LLD | Pd wt% (± 3σ) | Pd LLD | Pt wt% (± 3σ) | Pt LLD | Counts |
|---|---|---|---|---|---|---|---|
| **HU733** | 0.140 (0.014) | 0.012 | 0.051 (0.014) | 0.017 | 0.127 (0.020) | 0.019 | 200000 |
| **HU731** | | | | | 0.387 (0.026) | 0.011 | 200000 |

***Table 13.*** *Milli-PIXE trace element spot analyses of the melt phase that co-exists with nickel, equilibrated at 1100°C. Values in italics are statistically unreliable.*

| Exp | Rh wt% (± 3σ) | Rh LLD | Pd wt% (± 3σ) | Pd LLD | Pt wt% (± 3σ) | Pt LLD | Counts |
|---|---|---|---|---|---|---|---|
| **HU733** | 0.107 (0.013) | 0.017 | 0.082 (0.014) | 0.013 | 0.032 (0.015) | 0.024 | 200000 |
| **HU733** | 0.077 (0.013) | 0.017 | 0.125 (0.016) | 0.019 | *0.011* (0.016) | 0.028 | 200000 |
| **HU731** | | | | | 0.073 (0.016) | 0.025 | 200000 |
| **HU731** | | | | | 0.090 (0.016) | 0.023 | 200000 |

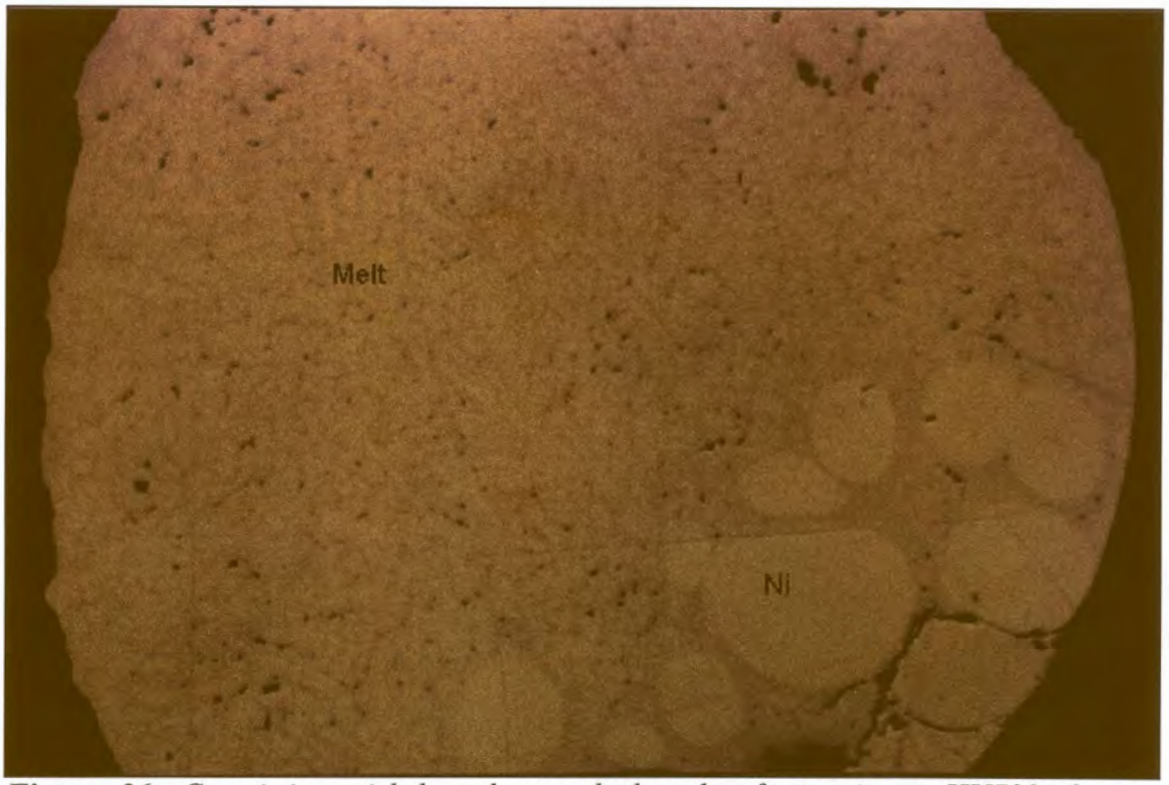


***Figure 36.*** *Co-existing nickel and quenched melt of experiment HU733 that was equilibrated at 1100°C. The experiment contained a bulk of 500 ppm each of Rh, Pd and Pt (exact amounts in Table A2; Appendix A). Field of view 4 mm.*

**5.1.1.2.1.2.** Results for equilibration at 1000°C

Two analyses were performed on the nickel in experiment HU381, and the average was used in further discussions (Table 20). The Pt value obtained in the analysis of melt in experiment HU393 (Table 15) is only just above the detection limit. This value was used for further calculations. The two analyses of the melt phase of experiment HU381 compare well (between 10 and 15 % variation for the three PGE), considering the associated errors. They were combined with resampling statistics (Table 20).

***Table 14.*** *Milli-PIXE trace element analyses of nickel that co-exists with melt, equilibrated at 1000°C.*

| Exp | Rh wt% (± 3σ) | Rh LLD | Pd wt% (± 3σ) | Pd LLD | Pt wt% (± 3σ) | Pt LLD | Counts |
|---|---|---|---|---|---|---|---|
| **HU393** | 0.391 (0.024) | 0.020 | 0.111 (0.020) | 0.031 | 0.555 (0.026) | 0.017 | 200000 |
| **HU381** | 0.869 (0.037) | 0.016 | 0.289 (0.025) | 0.019 | 1.387 (0.042) | 0.028 | 200000 |
| **HU381** | 0.907 (0.039) | 0.028 | 0.291 (0.027) | 0.026 | 1.322 (0.044) | 0.026 | 200000 |

***Table 15.*** *Milli-PIXE trace element analyses of the melt phases that co-exist with nickel, equilibrated at 1000°C.*

| Exp | Rh wt% (± 3σ) | Rh LLD | Pd wt% (± 3σ) | Pd LLD | Pt wt% (± 3σ) | Pt LLD | Counts |
|---|---|---|---|---|---|---|---|
| **HU393** | 0.141 (0.014) | 0.017 | 0.184 (0.017) | 0.014 | 0.025 (0.015) | 0.023 | 200000 |
| **HU381** | 0.198 (0.021) | 0.013 | 0.375 (0.030) | 0.034 | 0.047 (0.017) | 0.027 | 200000 |
| **HU381** | 0.249 (0.024) | 0.035 | 0.435 (0.030) | 0.024 | 0.058 (0.018) | 0.028 | 200000 |

**5.1.1.2.1.3.** Results for equilibration at 900°C

Two analyses were performed on the melt phase of experiment HU753 (Table 17). The Rh and Pd contents from the two analyses compare well, and the two analyses were combined with resampling statistics (Table 20). The Pt contents in both analyses were below detection, and the lowest detection limit was used in further calculations. The melt phase of experiment HU429 (Table 17) was analysed twice, and the two analyses vary considerably. From all the melt analyses it becomes clear that Pd is slightly concentrated in the melt phase, as opposed to Pt and Rh, which are concentrated in the nickel. However, in the second melt analysis of experiment HU429, the Rh content is almost the same as the Pd content, and therefore higher than would be expected. The Pt content is much higher than in the previous analysis. The calculated detection limits of all the elements are lower for the second analysis - more typical of a nickel analysis. Therefore, it is believed that this melt analysis was at least in part influenced by a hidden nickel phase that was not visible on the surface of the melt (penetration depth is discussed in section 4.2.). The second melt analysis was ignored in further discussions, and only the first analysis was used. The Pt detection limit was used further on.

***Table 16.*** *Milli-PIXE trace element analyses of nickel that co-exists with melt, equilibrated at 900°C.*

| Exp | Rh wt% (± 3σ) | Rh LLD | Pd wt% (± 3σ) | Pd LLD | Pt wt% (± 3σ) | Pt LLD | Counts |
|---|---|---|---|---|---|---|---|
| **HU753** | 0.374 (0.028) | 0.009 | 0.077 (0.022) | 0.021 | 0.332 (0.037) | 0.013 | 200000 |
| **HU429** | 0.737 (0.032) | 0.019 | 0.219 (0.023) | 0.030 | 0.778 (0.029) | 0.011 | 200000 |
| **HU427** | | | 0.304 (0.023) | 0.025 | | | 200000 |

***Table 17.*** *Milli-PIXE trace element analyses of the melt phases that co-exist with nickel equilibrated at 900°C. Values in italics are statistically unreliable.*

| Exp | Rh wt% (± 3σ) | Rh LLD | Pd wt% (± 3σ) | Pd LLD | Pt wt% (± 3σ) | Pt LLD | Counts |
|---|---|---|---|---|---|---|---|
| **HU753** | 0.081 (0.013) | 0.019 | 0.105 (0.019) | 0.018 | nd | 0.034 | 200000 |
| **HU753** | 0.102 (0.016) | 0.015 | 0.094 (0.019) | 0.032 | *0.020* (0.015) | 0.023 | 200000 |
| **HU429** | 0.134 (0.017) | 0.026 | 0.344 (0.024) | 0.024 | *0.006* (0.016) | 0.029 | 200000 |
| **HU429** | 0.236 (0.018) | 0.008 | 0.254 (0.022) | 0.018 | 0.038 (0.015) | 0.020 | 200000 |
| **HU427** | | | 0.352 (0.026) | 0.029 | | | 200000 |

**5.1.1.2.1.4.** Results for equilibration at 700°C

The melt phase of experiment HU471 was analysed twice, but Pt was below detection in both. For further calculations the lowest detection limit was used. The melt phase of experiment HU472 (Table 19) was analysed twice, but the second analysis was intended to be on the metal surface. After analysis of the sample the surface was microscopically investigated, and the analysis spots could be detected by the damage to the carbon coating of the sample. Both spots were found to be on the melt phase. The method used to orient the sample under the milli-PIXE beam was described in Section 4.2.1. and when the shape of a sample is not characteristic, it is difficult to find the intended position on the sample. Photograph 23 shows the position of the small nickel phase on the edge of the sample. The two melt analyses compare well, but due to the fact that no analysis was performed of the co-existing nickel in this experiment, it could not be used for further calculations.

All the milli-PIXE analyses that were used for further discussion are given in Table 20.

***Table 18***. *Milli-PIXE trace element analyses of nickel that co-exists with melt equilibrated at 700°C.*

| Exp | Rh wt% (± 3σ) | Rh LLD | Pd wt% (± 3σ) | Pd LLD | Pt wt% (± 3σ) | Pt LLD | Counts |
|---|---|---|---|---|---|---|---|
| **HU469** | 0.220 (0.022) | 0.017 | 0.032 (0.014) | 0.004 | 0.138 (0.023) | 0.036 | 200000 |
| **HU471** | | | | | 1.133 (0.043) | 0.024 | 200000 |
| **HU473** | 0.633 (0.043) | 0.034 | | | | | 200000 |

***Table 19***. *Milli-PIXE trace element analyses of the melt phases of experiments equilibrated at 700°C. Values in italics are statistically unreliable.*

| Exp | Rh wt% (± 3σ) | Rh LLD | Pd wt% (± 3σ) | Pd LLD | Pt wt% (± 3σ) | Pt LLD | Counts |
|---|---|---|---|---|---|---|---|
| **HU469** | 0.040 (0.010) | 0.013 | 0.062 (0.016) | 0.019 | *0.003* (0.016) | 0.028 | 200000 |
| **HU471** | | | | | *0.006* (0.024) | 0.044 | 200000 |
| **HU471** | | | | | nd | 0.046 | 200000 |
| **HU472** | | | 0.408 (0.039) | 0.045 | | | 200000 |
| **HU472** | | | 0.446 (0.035) | 0.027 | | | 200000 |
| **HU473** | 0.065 (0.027) | 0.046 | | | | | 200000 |

***Table 20***. *Milli-PIXE analyses of nickel and Ni-S melt in experiments of the Ni-S system. Values in italics are statistically unreliable.*

| Exp | Temp (°C) | Nickel | | | Quenched melt | | |
|---|---|---|---|---|---|---|---|
| | | Rh (wt%) | Pd (wt%) | Pt (wt%) | Rh (wt%) | Pd (wt%) | Pt (wt%) |
| **HU733** | 1100 | 0.140 | 0.051 | 0.127 | 0.092 | 0.104 | 0.032 |
| **HU731** | 1100 | | | 0.387 | | | 0.081 |
| **HU393** | 1000 | 0.391 | 0.111 | 0.555 | 0.141 | 0.184 | 0.025 |
| **HU381** | 1000 | 0.888 | 0.290 | 1.355 | 0.224 | 0.405 | 0.053 |
| **HU753** | 900 | 0.374 | 0.077 | 0.332 | 0.091 | 0.100 | <0.023 |
| **HU429** | 900 | 0.737 | 0.219 | 0.778 | 0.134 | 0.344 | <0.029 |
| **HU427** | 900 | | 0.304 | | | 0.352 | |
| **HU469** | 700 | 0.220 | 0.032 | 0.138 | 0.040 | 0.062 | <0.028 |
| **HU471** | 700 | | | 1.133 | | | <0.044 |
| **HU473** | 700 | 0.633 | | | 0.065 | | |

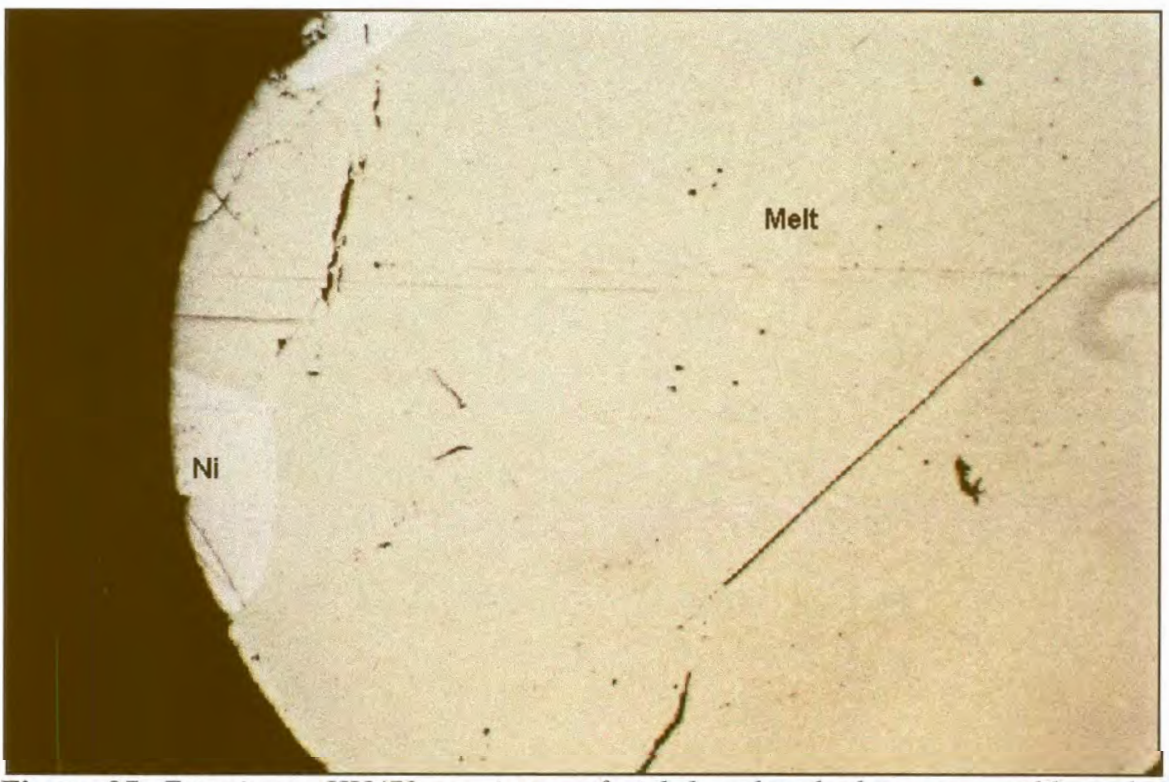


***Figure 37.*** *Experiment HU472 consisting of nickel and melt that was equilibrated at 700°C. The small area of nickel was not found during milli-PIXE analysis. Field of view 4 mm.*

#### 5.1.1.2.2. Micro-PIXE

##### 5.1.1.2.2.1. Results for equilibration at 1100°C

The small separated drop of melt of experiment HU441 was analysed separately by both EPMA (Section 5.1.1.1.) and PIXE (Table 22). The PGE content of the drop is very similar to the PGE content of the melt phase (Table 22), which implies that it separated from the charge after equilibration, possibly during quenching, as was discussed in section 5.1.1.1. The analysis of the separated drop was ignored in further calculations.

***Table 21.*** *Micro-PIXE trace element analyses of nickel that co-exists with melt equilibrated at 1100°C.*

| Exp | Rh wt% (± 3σ) | Rh LLD | Pd wt% (± 3σ) | Pd LLD | Pt wt% (± 3σ) | Pt LLD | Charge (nC) |
|---|---|---|---|---|---|---|---|
| **HU441** | 0.463 (0.020) | 0.008 | 0.087 (0.008) | 0.009 | 1.213 (0.029) | 0.020 | 54 |
| **HU437** | | | 0.103 (0.010) | 0.007 | | | 59 |

***Table 22.*** *Micro-PIXE trace element analyses of the melt phases that co-exist with nickel, equilibrated at 1100°C.*

| Exp | Rh wt% (± 3σ) | Rh LLD | Pd wt% (± 3σ) | Pd LLD | Pt wt% (± 3σ) | Pt LLD | Charge (nC) |
|---|---|---|---|---|---|---|---|
| **HU441** | 0.169 (0.011) | 0.004 | 0.183 (0.008) | 0.005 | 0.061 (0.006) | 0.010 | 106 |
| **HU441 drop** | 0.168 (0.008) | 0.005 | 0.176 (0.011) | 0.006 | 0.056 (0.006) | 0.013 | 79 |
| **HU437** | | | 0.142 (0.010) | 0.004 | | | 137 |

##### 5.1.1.2.2.2. Results for equilibration at 1000°C

Experiment HU392 was analysed by EPMA (Table 9) and described in section 5.1.1.1. It contained a separated drop that consists of nickel and quenched melt, while only quenched melt was observed in the rest of the charge. The metal analysis of experiment HU392 in Table 23 was performed on the separated drop (as no metal could be found in the main charge). The melt phases of both the main charge and the drop were analysed and the results are given in Table 24. From the table it is clear that the contents of all three PGE in

the melt phase of the main charge are significantly lower than in the melt phase of the drop, implying that the drop was separated from the main charge before complete equilibrium was reached. The bulk composition of the drop can, therefore, only be roughly guessed by extrapolation from the compositions of the metal and melt. It is not directly related to the initial composition of the entire charge (provided in Appendix A). As no metal could be found in the main charge, the analyses of the drop will be used as "experiment HU392" for further discussions, even though the composition does not correspond to the planned composition of the experiment. It is believed that equilibrium was achieved within the drop itself. Two PIXE analyses were performed on the melt phase of the drop, as the PGE content was low. With the GEOPIXE software package it is possible to add the counts of two analyses and obtain a result for the added counts. This corresponds to an analysis taken for the total of the counts which would be more reliable than either of the two analyses would be on their own. In Table 24, this analysis is presented as HU392 (sum), which was used in further discussion.

***Table 23.*** *Micro-PIXE trace element analyses of nickel that co-exists with melt, equilibrated at 1000°C.*

| Exp | Rh wt% (± 3σ) | Rh LLD | Pd wt% (± 3σ) | Pd LLD | Pt wt% (± 3σ) | Pt LLD | Charge (nC) |
|---|---|---|---|---|---|---|---|
| **HU393** | 0.349 (0.014) | 0.008 | 0.096 (0.013) | 0.009 | 0.737 (0.025) | 0.019 | 54 |
| **HU394** | 2.148 (0.044) | 0.014 | 0.493 (0.027) | 0.016 | 4.460 (0.093) | 0.029 | 30 |
| **HU395** | 3.197 (0.067) | 0.013 | 1.116 (0.043) | 0.015 | 6.351 (0.099) | 0.024 | 54 |
| **HU412** | 2.707 (0.051) | 0.009 | 0.761 (0.027) | 0.012 | 4.784 (0.076) | 0.022 | 60 |
| **HU392 drop** | 0.460 (0.016) | 0.008 | 0.044 (0.009) | 0.009 | 1.724 (0.034) | 0.210 | 50 |

The melt phase of experiment HU393 was analysed twice in an attempt to determine the low Pt content (Table 24). For the second analysis, a large number of counts was collected, lowering the detection limit and the error significantly. The two analyses compare well, but the second analysis will be used for further calculations, due to its smaller error and lower detection limit (Table 27).

Slightly less PGE were detected in the drop that accompanied experiment HU395, which implies slight concentration of PGE in the charge (Table 24), suggesting that the drop was separated before equilibrium conditions were reached. However, considering the large size of the charge compared to the small drop, it is concluded that the PGE concentration effect is negligible. The drop was not considered in further discussions.

***Table 24**. Micro-PIXE trace element analyses of the melt phases that co-exist with nickel equilibrated at 1000°C. Values in italics are statistically unreliable.*

| Exp | Rh wt% (± 3σ) | Rh LLD | Pd wt% (± 3σ) | Pd LLD | Pt wt% (± 3σ) | Pt LLD | Charge (nC) |
|---|---|---|---|---|---|---|---|
| **HU393** | 0.081 (0.004) | 0.002 | 0.136 (0.007) | 0.003 | 0.017 (0.002) | 0.007 | 300 |
| **HU393** | 0.075 (0.002) | 0.0004 | 0.124 (0.003) | 0.0005 | 0.015 (0.001) | 0.001 | 9579* |
| **HU394** | 0.489 (0.021) | 0.011 | 0.790 (0.030) | 0.013 | 0.098 (0.016) | 0.021 | 30 |
| **HU395** | 0.826 (0.028) | 0.007 | 1.760 (0.026) | 0.008 | 0.113 (0.006) | 0.012 | 89 |
| **HU395 drop** | 0.576 (0.014) | 0.005 | 1.327 (0.028) | 0.006 | 0.093 (0.005) | 0.010 | 115 |
| **HU412** | 0.719 (0.027) | 0.007 | 1.096 (0.027) | 0.009 | 0.107 (0.008) | 0.015 | 50 |
| **HU412 point** | 0.814 (0.020) | 0.006 | 1.081 (0.025) | 0.008 | 0.149 (0.007) | 0.013 | 72 |
| **HU392 drop** | 0.066 (0.006) | 0.004 | 0.042 (0.005) | 0.005 | *0.007* (0.004) | 0.011 | 100 |
| **HU392 drop** | 0.064 (0.003) | 0.003 | 0.050 (0.003) | 0.003 | *0.008* (0.004) | 0.008 | 200 |
| **HU392 sum** | 0.065 (0.003) | 0.002 | 0.048 (0.003) | 0.003 | 0.008 (0.003) | 0.006 | 300 |
| **HU392 main** | 0.005 (0.001) | 0.002 | 0.003 (0.002) | 0.002 | *0.002* (0.002) | 0.006 | 300 |

* ~10 hours

Two analyses were performed on the melt phase of experiment HU412 (Table 24). The first included an area on the melt (~ 100 x 100 μm), while the second was a point analysis on a spot with diameter of about 2 μm, ignoring the heterogeneity of the melt. The two analyses

do not differ much, possibly because the volume analysed by spot analysis is larger than the spot diameter itself. The area analysis was used for further discussion.

#### 5.1.1.2.2.3. Results for equilibration at 900°C

***Table 25.*** *Micro-PIXE trace element analyses of nickel that co-exists with melt, equilibrated at 900°C.*

| Exp | Rh wt% (± 3σ) | Rh LLD | Pd wt% (± 3σ) | Pd LLD | Pt wt% (± 3σ) | Pt LLD | Charge (nC) |
|---|---|---|---|---|---|---|---|
| **HU429** | 0.606 (0.020) | 0.007 | 0.151 (0.009) | 0.008 | 0.919 (0.020) | 0.019 | 65 |
| **HU426** | | | | | 0.360 (0.013) | 0.014 | 117 |
| **HU427** | | | 0.159 (0.008) | 0.004 | | | 163 |
| **HU428** | 0.596 (0.027) | 0.005 | | | | | 47 |

***Table 26.*** *Micro-PIXE trace element analyses of the melt phases that co-exist with nickel equilibrated at 900°C. Values in italics are statistically unreliable.*

| Exp | Rh wt% (± 3σ) | Rh LLD | Pd wt% (± 3σ) | Pd LLD | Pt wt% (± 3σ) | Pt LLD | Charge (nC) |
|---|---|---|---|---|---|---|---|
| **HU429** | 0.115 (0.004) | 0.002 | 0.225 (0.004) | 0.002 | 0.011 (0.002) | 0.005 | 510 |
| **HU426** | | | | | *0.004* (0.002) | 0.004 | 607 |
| **HU427** | | | 0.215 (0.008) | 0.003 | | | 181 |
| **HU427 drop** | | | *0.001* (0.002) | 0.004 | | | 99 |
| **HU428** | 0.110 (0.004) | 0.003 | | | | | 173 |

All the PGE contents determined by micro-PIXE analysis that were used for further discussion are presented in Table 27. Values in italics indicate analyses where errors and background were very high compared to the PGE content.

***Table 27.*** *Results of micro-PIXE analyses of nickel and Ni-S-melt in experiments of the Ni-S system. Values in italics are statistically unreliable.*

| Exp | Temp (°C) | Nickel | | | Quenched melt | | |
|---|---|---|---|---|---|---|---|
| | | Rh (wt%) | Pd (wt%) | Pt (wt%) | Rh (wt%) | Pd (wt%) | Pt (wt%) |
| **HU441** | 1100 | 0.463 | 0.087 | 1.213 | 0.169 | 0.183 | 0.061 |
| **HU437** | 1100 | | 0.103 | | | 0.142 | |
| **HU393** | 1000 | 0.349 | 0.096 | 0.737 | 0.075 | 0.124 | 0.015 |
| **HU394** | 1000 | 2.148 | 0.493 | 4.460 | 0.489 | 0.790 | 0.098 |
| **HU395** | 1000 | 3.197 | 1.116 | 6.351 | 0.826 | 1.760 | 0.113 |
| **HU412** | 1000 | 2.707 | 0.761 | 4.784 | 0.719 | 1.096 | 0.107 |
| **HU392** | 1000 | 0.460 | 0.044 | 1.724 | 0.065 | 0.048 | 0.008 |
| **HU429** | 900 | 0.606 | 0.151 | 0.919 | 0.115 | 0.225 | 0.011 |
| **HU426** | 900 | | | 0.360 | | | *0.004* |
| **HU427** | 900 | | 0.159 | | | 0.215 | |
| **HU428** | 900 | 0.596 | | | 0.110 | | |

## 5.2. The Cu-S system

### 5.2.1. Cu-rich melt - S-rich melt assemblage (1200°C)

#### 5.2.1.1. EPMA results

The major element compositions of the quenched Cu-rich and S-rich melts determined by EPMA are given in Table 28, and projected onto the phase diagram of the Cu-S system (after Chakrabarti and Laughlin, 1986) at 1200°C (Figure 15 – blue triangles). These compositions compare favourably with the expected compositions.

***Table 28**. Major element compositions, determined by EPMA, of co-existing Cu-rich melt and S-rich melt equilibrated at 1200°C.*

| Exp | Phase | Cu wt% (± 3σ) | S wt% (± 3σ) | Total (wt%) | PGE# (wt%) | n |
|---|---|---|---|---|---|---|
| **HU442** | Cu-rich melt | 97.63 (0.36) | 1.03 (0.26) | 98.66 | ~0.8 | 39 |
| | S-rich melt | 80.21 (0.90) | 19.84 (0.69) | 100.05 | <0.1 | 30 |
| **HU443** | Cu-rich melt | 97.92 (0.50) | 1.04 (0.37) | 98.96 | ~0.3 | 30 |
| | S-rich melt | 79.24 (0.89) | 20.03 (0.25) | 99.27 | <0.1 | 16 |
| **HU444** | Cu-rich melt | 98.34 (0.80) | 1.08 (0.35) | 99.42 | ~0.4 | 29 |
| | S-rich melt | 80.10 (0.50) | 19.43 (0.45) | 99.53 | ~0.05 | 52 |
| **HU445** | Cu-rich melt | 99.05 (0.51) | 1.16 (0.33) | 100.21 | ~0.4 | 38 |
| | S-rich melt | 80.22 (0.89) | 19.52 (1.00) | 99.74 | <0.01 | 38 |
| **HU450** | Cu-rich melt | 97.30 (0.45) | 1.17 (0.40) | 98.47 | ~0.8 | 35 |
| | S-rich melt | 79.33 (0.46) | 19.97 (0.38) | 99.30 | <0.1 | 38 |

# = Estimation of total PGE content as determined by PIXE, discussed in section 5.2.1.2.

### 5.2.1.2. PIXE results

#### 5.2.1.2.1. Milli-PIXE

##### 5.2.1.2.1.1. Results for equilibration at 1200°C

Very low detection limits were obtained for all three PGE in the Cu-rich melt of experiment HU442, because three times the normal number of counts were collected. The detection limits for the other experiments are much higher. The Cu-rich melt in experiment HU443 was analysed twice, the two results compare well, and were combined with resampling statistics (Table 31). In experiment HU444 two analyses were combined with resampling statistics.

***Table 29.*** *Milli-PIXE trace element analyses of the Cu-rich melt phase co-existing with the S-rich melt phase equilibrated at 1200°C.*

| Exp | Rh wt% (± 3σ) | Rh LLD | Pd wt% (± 3σ) | Pd LLD | Pt wt% (± 3σ) | Pt LLD | Counts |
|---|---|---|---|---|---|---|---|
| **HU442** | 0.238 (0.013) | 0.016 | 0.324 (0.016) | 0.013 | 0.265 (0.022) | 0.031 | 600000 |
| **HU443** | | | | | 0.359 (0.036) | 0.053 | 200000 |
| **HU443** | | | | | 0.330 (0.037) | 0.055 | 200000 |
| **HU444** | | | 0.366 (0.028) | 0.032 | | | 200000 |
| **HU444** | | | 0.428 (0.028) | 0.021 | | | 200000 |
| **HU445** | 0.384 (0.026) | 0.025 | | | | | 200000 |
| **HU450** | 0.364 (0.025) | 0.022 | 0.241 (0.021) | 0.021 | 0.173 (0.032) | 0.044 | 200000 |

The S-rich melt of experiment HU442 was analysed twice. In both cases the Rh and Pt contents were below the detection limits, and the lowest detection limits were used in further calculations. Pd could be detected in both analyses, because the detection limits at the Pd peak positions were much lower than for Rh and Pt. Resampling statistics was used to combine the analyses. Out of the seven analyses on the S-rich melt of experiment HU443, Pt was detected only during the second. This higher than expected Pt peak could indicate interference from the Cu-rich melt, or heterogeneity of the melt. Whatever the reason, this result is inconsistent with the other analyses, and will therefore be ignored. The fourth analysis was left to collect more counts than any of the other analyses, and obtained the lowest detection limit, which was used in further calculations. The S-rich melt of experiment HU444 was analysed three times. The analysis for which most counts was collected (200000) was the only one where Pd could be detected, and this was used for further calculations. The S-rich melt of experiment HU445 was analysed twice, and the second time twice as many counts were collected, resulting in a lower detection limit, which was used for further calculations. The peaks of all three PGE were found to be below detection in the S-rich melt of experiment HU450.

***Table 30***. *Milli-PIXE trace element analyses of the S-rich melt phases co-existing with Cu-rich melt phases, equilibrated at 1200°C. Values in italics are statistically unreliable.*

| Exp | Rh wt% (± 3σ) | Rh LLD | Pd wt% (± 3σ) | Pd LLD | Pt wt% (± 3σ) | Pt LLD | Counts |
|---|---|---|---|---|---|---|---|
| **HU442** | bd | 0.026 | 0.022 (0.009) | 0.017 | *0.021* (0.026) | 0.044 | 200000 |
| **HU442** | bd | 0.029 | 0.026 (0.011) | 0.014 | bd | 0.052 | 200000 |
| **HU443** | | | | | *0.003* (0.026) | 0.048 | 200000 |
| **HU443** | | | | | 0.063 (0.024) | 0.034 | 200000 |
| **HU443** | | | | | bd | 0.057 | 200000 |
| **HU443** | | | | | *0.015* (0.018) | 0.031 | 400000 |
| **HU443** | | | | | *0.036* (0.032) | 0.053 | 100000 |
| **HU443** | | | | | *0.024* (0.030) | 0.053 | 100000 |
| **HU443** | | | | | *0.007* (0.037) | 0.067 | 100000 |
| **HU444** | | | bd | 0.122 | | | 100000 |
| **HU444** | | | 0.053 (0.015) | 0.018 | | | 200000 |
| **HU444** | | | bd | 0.026 | | | 170000 |
| **HU445** | bd | 0.024 | | | | | 200000 |
| **HU445** | *0.009* (0.007) | 0.011 | | | | | 400000 |
| **HU450** | *0.011* (0.009) | 0.017 | bd | 0.038 | bd | 0.053 | 200000 |

***Table 31***. *Results of milli-PIXE analyses of Cu-rich melt and S-rich melt in experiments of the Cu-S system.*

| Exp | Temp (°C) | Cu-rich melt | | | S-rich melt | | |
|---|---|---|---|---|---|---|---|
| | | Rh (wt%) | Pd (wt%) | Pt (wt%) | Rh (wt%) | Pd (wt%) | Pt (wt%) |
| **HU442** | 1200 | 0.238 | 0.324 | 0.265 | <0.026 | 0.024 | <0.044 |
| **HU443** | 1200 | | | 0.345 | | | <0.031 |
| **HU444** | 1200 | | 0.397 | | | 0.053 | |
| **HU445** | 1200 | 0.384 | | | <0.011 | | |
| **HU450** | 1200 | 0.364 | 0.241 | 0.173 | <0.017 | <0.038 | <0.053 |

### 5.2.2. Copper - digenite assemblage (1000°C and 800°C)

#### 5.2.2.1. EPMA results

Tables 32 and 33 contain the major element compositions as determined by EPMA of the co-existing copper and digenite equilibrated at 1000°C and 800°C. These compositions are also shown on the phase diagram of the Cu-S system (Figure 15 – pink triangles), where the determined compositions are projected on the Cu-S phase diagram, and can be compared to the expected compositions of the phases according to Chakrabarti and Laughlin (1986).

#### 5.2.2.2. PIXE results

##### 5.2.2.2.1. Milli-PIXE

###### 5.2.2.2.1.1. Results for equilibration at 1000°C

The copper of experiment HU384 was analysed twice, and the analyses were combined with resampling statistics. The copper phase of experiment HU385 was analysed three times, but more counts were collected for the last two, with resulting lower detection limits. The last two analyses were combined with resampling statistics and are used for further discussion. The low Pt content detected in the metal of experiment HU387 and the low Pd content in the metal of experiment HU417 are unusual in comparison with the analyses of the other experiments. The reason for this is unknown.

The lowest detection limit for Pt in digenite of experiment HU382, Rh in digenite of experiment HU384, and Rh, Pd and Pt in digenite of experiment HU385, were used for further discussion. Two analyses were performed on the digenite of experiment HU387, and although the analytical conditions were exactly the same during both analyses, lower detection were obtained from the second analysis, which was used for further discussion. Only a detection limit could be obtained for the Pd in the digenite of experiment HU417, and as only a detection limit is available for Pd in the co-existing metal in this experiment as

well, the results cannot be used for further calculations. The second analysis of the digenite of experiment HU465 was used.

***Table 32.*** *Major element compositions, determined by EPMA, of co-existing copper and digenite equilibrated at 1000°C.*

| Exp | Phase | Cu wt% (± 3σ) | S wt% (± 3σ) | Total (wt%) | PGE# (wt%) | n |
|---|---|---|---|---|---|---|
| **HU382** | Copper | 98.63 (0.31) | bd | 98.63 | ~0.7 | 28 |
| | Digenite | 79.25 (0.43) | 19.90 (0.16) | 99.15 | ~0.05 | 30 |
| **HU384** | Copper | 98.52 (0.29) | bd | 98.52 | ~0.9 | 25 |
| | Digenite | 79.38 (0.39) | 19.82 (0.19) | 99.20 | <0.1 | 34 |
| **HU385** | Copper | 97.79 (0.18) | bd | 97.79 | ~1.7 | 39 |
| | Digenite | 79.35 (0.38) | 20.11 (0.18) | 99.46 | <0.1 | 38 |
| **HU387** | Copper | 99.55 (0.50) | 0.05 (0.06) | 99.55 | ~0.9 | 22 |
| | Digenite | 79.97 (0.30) | 20.19 (0.18) | 100.16 | <0.1 | 30 |
| **HU417** | Copper | 98.66 (0.26) | bd | 98.66 | bd | 20 |
| | Digenite | 78.91 (0.47) | 20.34 (0.19) | 99.25 | bd | 22 |
| **HU465** | Copper | 93.63 (0.27) | bd | 93.63 | ~7.9 | 30 |
| | Digenite | 79.53 (0.55) | 20.47 (0.31) | 100.00 | <0.1 | 35 |

# = Estimation of total PGE content as determined by PIXE, discussed in section 5.2.2.2.

***Table 33.*** *Major element compositions, determined by EPMA, of co-existing copper and digenite equilibrated at 800°C.*

| Exp | Phase | Cu wt% (± 3σ) | S wt% (± 3σ) | Total (wt%) | PGE# (wt%) | n |
|---|---|---|---|---|---|---|
| **HU482** | Copper | 99.10 (0.50) | bd | 99.10 | 3.4 | 24 |
| | Digenite | 80.18 (1.17) | 19.97 (0.81) | 100.15 | <0.1 | 48 |
| **HU483** | Copper | 99.12 (0.70) | bd | 99.12 | nd | 35 |
| | Digenite | 79.05 (0.43) | 20.35 (0.19) | 99.40 | nd | 38 |
| **HU484** | Copper | 99.98 (0.61) | bd | 99.98 | nd | 63 |
| | Digenite | 80.09 (0.69) | 20.09 (0.27) | 100.18 | nd | 53 |
| **HU485** | Copper | 99.91 (0.89) | bd | 99.91 | nd | 30 |
| | Digenite | 80.08 (0.84) | 19.46 (0.95) | 99.54 | nd | 52 |

# = Estimation of total PGE content as determined by PIXE, discussed in section 5.2.2.2.

***Table 34***. *Milli-PIXE trace element analyses of copper that co-exists with digenite, equilibrated at 1000°C. Values in italics are statistically unreliable.*

| Exp | Rh wt% (± 3σ) | Rh LLD | Pd wt% (± 3σ) | Pd LLD | Pt wt% (± 3σ) | Pt LLD | Counts |
|---|---|---|---|---|---|---|---|
| **HU382** | | | | | 0.704 (0.044) | 0.024 | 140000 |
| **HU384** | 0.972 (0.058) | 0.053 | | | | | 100000 |
| **HU384** | 0.905 (0.056) | 0.057 | | | | | 100000 |
| **HU385** | 0.386 (0.040) | 0.048 | 1.054 (0.063) | 0.048 | 0.590 (0.056) | 0.060 | 100000 |
| **HU385** | 0.465 (0.030) | 0.026 | 0.896 (0.040) | 0.040 | 0.584 (0.042) | 0.058 | 200000 |
| **HU385** | 0.395 (0.027) | 0.029 | 0.741 (0.037) | 0.038 | 0.443 (0.037) | 0.041 | 200000 |
| **HU387** | 0.376 (0.027) | 0.025 | 0.487 (0.031) | 0.021 | *0.060* (0.036) | 0.061 | 200000 |
| **HU417** | | | *0.005* (0.012) | 0.023 | | | 200000 |
| **HU417** | | | bd | 0.041 | | | 200000 |
| **HU465** | 2.177 (0.070) | 0.058 | 3.691 (0.084) | 0.065 | 2.002 (0.068) | 0.064 | 200000 |

***Table 35***. *Milli-PIXE trace element analyses of digenite that co-exists with copper, equilibrated at 1000°C. Values in italics are statistically unreliable.*

| Exp | Rh wt% (± 3σ) | Rh LLD | Pd wt% (± 3σ) | Pd LLD | Pt wt% (± 3σ) | Pt LLD | Counts |
|---|---|---|---|---|---|---|---|
| **HU382** | | | | | bd | 0.087 | 100000 |
| **HU382** | | | | | bd | 0.047 | 200000 |
| **HU384** | bd | 0.028 | | | | | 200000 |
| **HU384** | bd | 0.047 | | | | | 200000 |
| **HU384** | *0.007* (0.009) | 0.016 | | | | | 200000 |
| **HU385** | *0.014* (0.009) | 0.016 | bd | 0.032 | bd | 0.052 | 200000 |
| **HU385** | bd | 0.018 | bd | 0.028 | bd | 0.038 | 300000 |
| **HU387** | bd | 0.023 | bd | 0.035 | bd | 0.052 | 200000 |
| **HU387** | bd | 0.025 | 0.022 (0.011) | 0.016 | *0.003* (0.027) | 0.049 | 200000 |
| **HU417** | | | *0.012* (0.016) | 0.032 | | | 200000 |
| **HU465** | bd | 0.026 | 0.040 (0.011) | 0.019 | *0.020* (0.022) | 0.038 | 200000 |
| **HU465** | *0.006* (0.007) | 0.013 | 0.037 (0.009) | 0.014 | *0.022* (0.021) | 0.036 | 400000 |

#### 5.2.2.2.1.2. Results for equilibration at 800°C

The second of the two analyses on the digenite of experiment HU482 was used in further calculations.

***Table 36.*** *Milli-PIXE trace element analysis of copper that co-exists with digenite, equilibrated at 800°C.*

| Exp | Rh wt% (± 3σ) | Rh LLD | Pd wt% (± 3σ) | Pd LLD | Pt wt% (± 3σ) | Pt LLD | Counts |
|---|---|---|---|---|---|---|---|
| **HU482** | 1.131 (0.045) | 0.038 | 1.171 (0.047) | 0.026 | 1.143 (0.055) | 0.045 | 200000 |

***Table 37.*** *Milli-PIXE trace element analyses of the digenite that co-exists with copper, equilibrated at 800°C.*

| Exp | Rh wt% (± 3σ) | Rh LLD | Pd wt% (± 3σ) | Pd LLD | Pt wt% (± 3σ) | Pt LLD | Counts |
|---|---|---|---|---|---|---|---|
| **HU482** | bd | 0.031 | bd | 0.034 | bd | 0.048 | 200000 |
| **HU482** | 0.025 (0.010) | 0.013 | bd | 0.027 | bd | 0.053 | 200000 |

***Table 38.*** *Results of milli-PIXE analyses of the copper - digenite assemblage in experiments of the Cu-S system.*

| Exp | Temp (°C) | Copper | | | Digenite | | |
|---|---|---|---|---|---|---|---|
| | | Rh (wt%) | Pd (wt%) | Pt (wt%) | Rh (wt%) | Pd (wt%) | Pt (wt%) |
| **HU382** | 1000 | | | 0.704 | | | <0.047 |
| **HU384** | 1000 | 0.939 | | | <0.016 | | |
| **HU385** | 1000 | 0.430 | 0.819 | 0.514 | <0.018 | <0.028 | <0.038 |
| **HU387** | 1000 | 0.376 | 0.487 | <0.061 | <0.025 | 0.022 | <0.049 |
| **HU465** | 1000 | 2.177 | 3.691 | 2.002 | <0.013 | 0.037 | <0.036 |
| **HU482** | 800 | 1.131 | 1.171 | 1.143 | 0.025 | <0.027 | <0.053 |

#### 5.2.2.2.2. Micro-PIXE

##### 5.2.2.2.2.1. Results for equilibration at 1000°C

***Table 39.*** *Micro-PIXE trace element analysis of copper that co-exists with digenite, equilibrated at 1000°C.*

| Exp | Rh wt% (± 3σ) | Rh LLD | Pd wt% (± 3σ) | Pd LLD | Pt wt% (± 3σ) | Pt LLD | Charge (nC) |
|---|---|---|---|---|---|---|---|
| **HU385** | 0.353 (0.014) | 0.009 | 0.600 (0.027) | 0.011 | 0.543 (0.020) | 0.032 | 54 |

The PGE content in the digenite is so low that no peaks could be detected during a first analysis. The second analysis of this phase was left to collect much more charge, but the Rh peak was still lower than the detection limit. The Pd and Pt peaks were above the detection limits, and will be used for further calculations.

***Table 40.*** *Micro-PIXE trace element analyses of digenite that co-exists with copper, equilibrated at 1000°C. Values in italics are statistically unreliable.*

| Exp | Rh wt% (± 3σ) | Rh LLD | Pd wt% (± 3σ) | Pd LLD | Pt wt% (± 3σ) | Pt LLD | Charge (nC) |
|---|---|---|---|---|---|---|---|
| **HU385** | bd | bd | *0.001* (0.002) | 0.004 | bd | bd | 165 |
| **HU385** | *0.0004* (0.0002) | 0.0006 | 0.0009 (0.0003) | 0.0007 | 0.0026 (0.0055) | 0.0021 | 5097 |

***Table 41.*** *Results of micro-PIXE analyses of the copper - digenite assemblage in experiments of the Cu-S system.*

| Exp | Temp (°C) | Copper | | | Digenite | | |
|---|---|---|---|---|---|---|---|
| | | Rh (wt%) | Pd (wt%) | Pt (wt%) | Rh (wt%) | Pd (wt%) | Pt (wt%) |
| **HU385** | 1000 | 0.353 | 0.600 | 0.543 | <0.0006 | 0.0009 | 0.0026 |

### 5.2.3. Digenite – Cu-S melt assemblage (1000°C)

#### 5.2.3.1. EPMA results

Table 42 presents the major element compositions of co-existing digenite and melt that were equilibrated at 1000°C. The compositions are projected onto the Cu-S phase diagram at 1000°C, and can be compared to the compositions expected from published phase diagrams (Figure 15 – green triangles; Figure 16 – blue and green triangles). The determined compositions of both digenite and melt are very similar, with overlapping error bars as shown on the phase diagram. It is possible that the two phases, which are optically very similar, are closely inter-grown, and that the analysed areas frequently consisted of not only the intended phase but rather a mixture of both phases.

***Table 42.*** *Major element compositions, determined by EPMA, of co-existing melt and digenite equilibrated at 1000°C.*

| Exp | Phase | Cu wt% (± 3σ) | S wt% (± 3σ) | Total (wt%) | PGE# (wt%) | n |
|---|---|---|---|---|---|---|
| **HU397** | Melt | 77.34 (0.33) | 22.16 (0.14) | 99.50 | ~2.3 | 19 |
| | Digenite | 78.18 (0.44) | 22.06 (0.39) | 100.24 | ~0.4 | 32 |
| **HU398** | Melt | 76.91 (0.38) | 21.64 (0.13) | 98.55 | ~4.4 | 16 |
| | Digenite | 78.80 (0.60) | 21.54 (0.57) | 100.34 | ~0.8 | 34 |
| **HU411** | Melt | 76.49 (0.71) | 22.95 (0.15) | 99.44 | ~3.5 | 22 |
| | Digenite | 78.24 (0.49) | 22.17 (0.40) | 100.41 | ~0.2 | 54 |
| **HU413** | Melt | 77.86 (0.31) | 22.96 (0.12) | 100.82 | ~1.7 | 7 |
| | Digenite | 78.56 (0.32) | 22.39 (0.27) | 100.95 | ~0.1 | 25 |
| **HU418** | Melt | 77.59 (0.50) | 22.23 (0.27) | 99.82 | ~0.5 | 27 |
| | Digenite | 78.08 (0.25) | 22.53 (0.20) | 100.61 | <0.1 | 22 |
| **HU420** | Melt | 77.39 (0.47) | 22.64 (0.29) | 100.03 | ~0.2 | 48 |
| | Digenite | 78.23 (0.36) | 22.04 (0.32) | 100.27 | <0.1 | 26 |

# Estimation of total PGE content as determined by PIXE, discussed in section 5.2.3.2.

#### 5.2.3.1.1. Separated drop

A separated drop, consisting of bright subhedral crystals in a heterogeneous matrix of lower reflectivity, was found with experiment HU397. The longest axis of the drop, shown in Figure 38, is about 3 mm. Experiment HU397, shown in Figure 39, consists of digenite and melt equilibrated at 1000°C. The separated drop differs significantly from the main charge. EPMA analyses (20 spot analyses) were performed on the two phases in the drop to determine the Cu, S, Rh, Pd and Pt contents. Accordingly, the bright crystals contain 13.95 wt% Cu ($1\sigma = 0.16$ wt%), 28.67 wt% S ($1\sigma = 0.30$ wt%), 28.85 wt% Rh ($1\sigma = 0.29$ wt%), and 28.87 wt% Pt ($1\sigma = 0.25$ wt%). This corresponds to 14.24 at% Cu, 57.99 at% S, 18.18 at% Rh and 9.60 at% Pt, with a proposed empirical formula of $Cu(Rh,Pt)_2S_4$. The formula lies between those of malanite ($CuPt_2S_4$) and cuprorhodsite ($CuRh_2S_4$), but due to the Rh:Pt atomic ratio of close to 2:1, would be classified as cuprorhodsite (Rudashevskiy *et al.* 1984; Rudashevskiy *et al.* 1985; Kolonin *et al.*, 1997). The atomic ratio of 2:1 of Rh to Pt corresponds to the ratio in which these elements were added to the experiment. No Pd could be detected in the crystals. The matrix was analysed with 40 µm diameter beam spots in order to compensate for the uneven texture, but the phase is very heterogeneous. According to ten analyses, it consists of 2.67 wt% Pt ($1\sigma = 0.52$ wt%), 15.10 wt% Rh ($1\sigma = 5.41$ wt%), 5.51 wt% Pd ($1\sigma = 1.05$ wt%), 52.22 wt% Cu ($1\sigma = 7.56$ wt%) and 22.47 wt% S ($1\sigma = 0.38$ wt%). If equilibrium was obtained in the drop, this implies that Pt, followed by Rh, and to a lesser extent S, were concentrated in the crystals, while Cu and Pd preferentially remained in the melt.

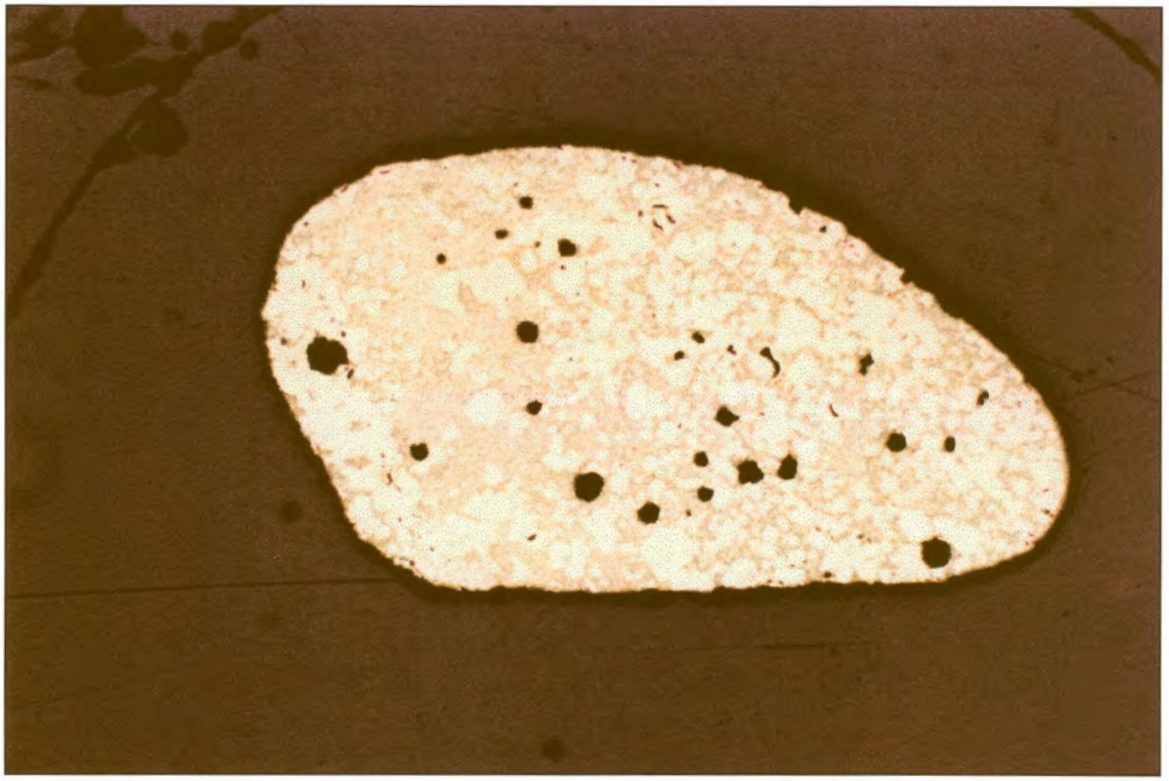

***Figure 38.*** *The separated drop from experiment HU397. Bright subhedral crystals (Cu, S, Rh, Pt) and a highly heterogeneous matrix can be distinguished. Image was digitally enhanced. Field of view 4 mm.*

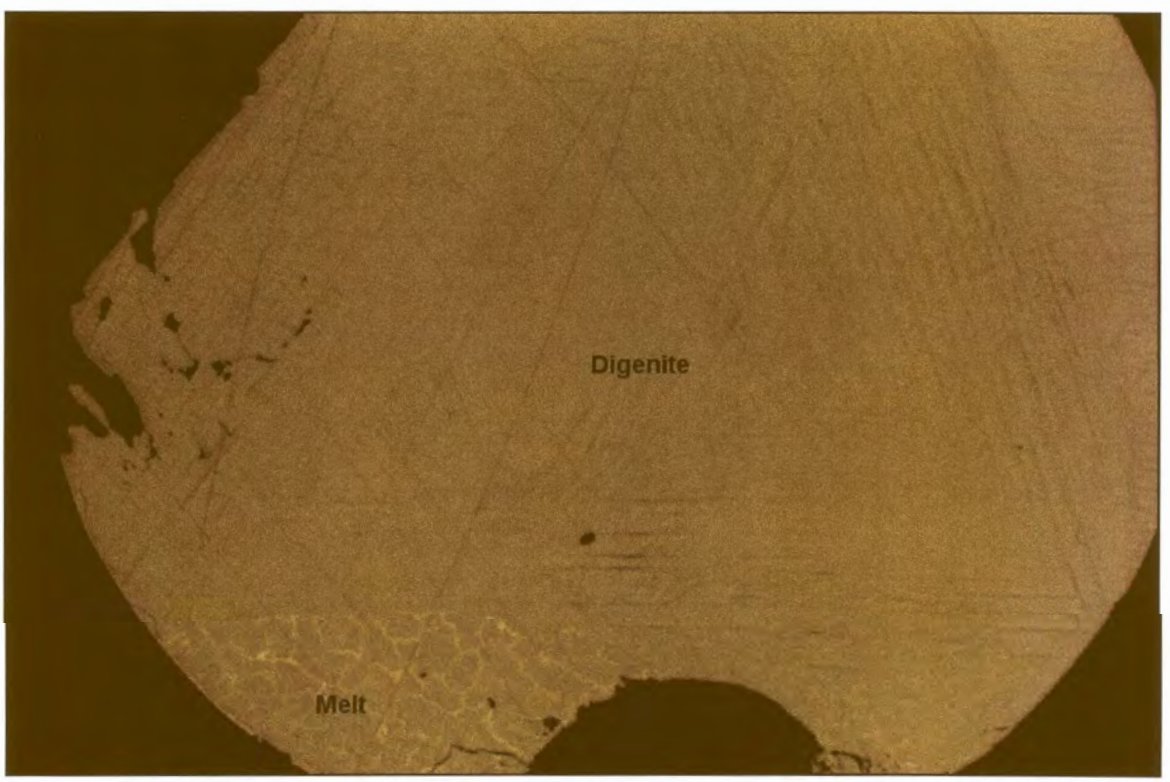


***Figure 39.*** *Experiment HU397 that consists of co-existing digenite and melt. The experiment was equilibrated at 1000°C. Image was digitally enhanced. Field of view 4 mm.*

### 5.2.3.2. PIXE results

#### 5.2.3.2.1. Micro-PIXE

##### 5.2.3.2.1.1. Results for equilibration at 1000°C

The Rh contents of experiment HU397 in both the digenite and the melt are very low, and Rh was probably concentrated in the separated drop (EPMA results section 5.2.3.1. and Figure 38). Similarly, for experiment HU398, the Rh content in both the digenite and the melt is very low, but no separated drop or separated alloy was found in the experiment.

***Table 43.*** *Micro-PIXE trace element analyses of digenite co-existing with melt, equilibrated at 1000°C.*

| Exp | Rh wt% (± 3σ) | Rh LLD | Pd wt% (± 3σ) | Pd LLD | Pt wt% (± 3σ) | Pt LLD | Charge (nC) |
|---|---|---|---|---|---|---|---|
| **HU397** | 0.004 (0.002) | 0.003 | 0.397 (0.010) | 0.004 | 0.023 (0.008) | 0.013 | 165 |
| **HU398** | 0.015 (0.003) | 0.005 | 0.668 (0.015) | 0.006 | 0.148 (0.016) | 0.016 | 102 |
| **HU398** | 0.014 (0.003) | 0.005 | 0.659 (0.023) | 0.006 | 0.127 (0.008) | 0.019 | 85 |
| **HU411** | 0.051 (0.002) | 0.002 | 0.136 (0.005) | 0.003 | 0.033 (0.005) | 0.008 | 414 |
| **HU413** | 0.021 (0.001) | 0.002 | 0.055 (0.003) | 0.002 | 0.014 (0.005) | 0.007 | 503 |
| **HU418** | | | | | 0.043 (0.005) | 0.009 | 307 |
| **HU420** | 0.024 (0.003) | 0.003 | | | | | 164 |

***Table 44.*** *Micro-PIXE trace element analyses of melt co-existing with digenite, equilibrated at 1000°C.*

| Exp | Rh wt% (± 3σ) | Rh LLD | Pd wt% (± 3σ) | Pd LLD | Pt wt% (± 3σ) | Pt LLD | Charge (nC) |
|---|---|---|---|---|---|---|---|
| **HU397** | 0.014 (0.003) | 0.005 | 1.890 (0.020) | 0.006 | 0.393 (0.013) | 0.013 | 150 |
| **HU397 (drop)** | 1.232 (0.018) | 0.004 | 0.145 (0.008) | 0.005 | 1.408 (0.029) | 0.008 | 101 |
| **HU398** | 0.091 (0.008) | 0.009 | 2.645 (0.075) | 0.011 | 1.743 (0.049) | 0.025 | 50 |
| **HU411** | 2.199 (0.034) | 0.009 | 0.548 (0.024) | 0.011 | 0.777 (0.018) | 0.020 | 74 |
| **HU413** | 1.317 (0.034) | 0.008 | 0.159 (0.009) | 0.009 | 0.199 (0.009) | 0.019 | 70 |
| **HU418** | | | | | 0.546 (0.014) | 0.018 | 87 |
| **HU420** | 0.234 (0.011) | 0.004 | | | | | 108 |

***Table 45**. Results of micro-PIXE analyses of the digenite - melt assemblage in experiments of the Cu-S system.*

| Exp | Temp | Digenite | | | Melt | | |
|---|---|---|---|---|---|---|---|
| | (°C) | Rh (wt%) | Pd (wt%) | Pt (wt%) | Rh (wt%) | Pd (wt%) | Pt (wt%) |
| **HU397** | 1000 | 0.004 | 0.397 | 0.023 | 0.014 | 1.890 | 0.393 |
| **HU398** | 1000 | 0.015 | 0.664 | 0.138 | 0.091 | 2.645 | 1.743 |
| **HU411** | 1000 | 0.051 | 0.136 | 0.033 | 2.199 | 0.548 | 0.777 |
| **HU413** | 1000 | 0.021 | 0.055 | 0.014 | 1.317 | 0.159 | 0.199 |
| **HU418** | 1000 | | | 0.043 | | | 0.546 |
| **HU420** | 1000 | 0.024 | | | 0.234 | | |

## 5.3 The Fe-S (±O) system

The majority of the quartz tubes containing the Fe-S experiments cracked during heating which led to the frequent oxidation of experiments. This was probably due to poor quality of the quartz glass tubes. Where oxygen was present during equilibration, the system concerned is no longer the Fe-S system but the Fe-S-O system. Oxygen could not be measured with the available EPMA or PIXE instrumentation. Except for a few qualitative SEM analyses, oxygen was not determined. Some of the experiments were severely contaminated with oxygen (mostly those containing the metal-melt assemblage), others contained less oxygen (the pyrrhotite-melt assemblages), while some appeared not to have been contaminated (metal-troilite assemblages). Oxygen was present in the form of oxides in the experiments. The state of oxidation of individual experiments will be discussed.

A number of precautions were taken to prevent oxidation of the experiments. Longer reduction time of the metallic Fe at a variety of temperatures and $H_2$ pressures before weighing-in showed no decrease in failure rate. Experiments were also pre-reacted at lower temperatures for longer than normal, and the period of equilibration at high temperatures was limited. Resealing of experiments in new tubes as soon as signs of weakening of the glass, with subsequent cracking, became apparent, also did not help. Due to these technical

problems, the Fe-S system could not be investigated comprehensively. Only a few exploratory investigations are reported on.

### 5.3.1. Iron – Fe-S melt assemblage (1200°C to 1000°C)

#### 5.3.1.1. EPMA results

The major element compositions of the co-existing iron and melt, as determined by EPMA, for the experiments at 1200°C, 1100°C and 1000°C are given in Tables 46 to 48.

***Table 46.*** *Major element compositions, determined by EPMA, of co-existing iron and quenched melt (containing O) equilibrated at 1200°C.*

| Exp | Phase | Fe wt% (± 3σ) | S wt% (± 3σ) | Total (wt%) | PGE# (wt%) | n |
|---|---|---|---|---|---|---|
| **HU825** | Iron | 91.92 (1.78) | bd | **91.92 | ~14.1 | 30 |
| | Melt | 62.05 (1.10) | 29.43 (1.41) | *91.48 | ~0.05 | 24 |
| **HU826** | Iron | 99.77 (0.36) | bd | 99.77 | ~0.2 | 20 |
| | Melt | 66.21 (2.35) | 28.68 (1.89) | *94.89 | ~0.3 | 20 |
| **HU827** | Iron | 99.44 (0.30) | bd | 99.44 | ~0.5 | 20 |
| | Melt | 62.55 (0.97) | 32.18 (1.03) | *94.73 | ~0.1 | 20 |

\# estimation of total PGE content as determined by PIXE, discussed in section 5.3.1.2.

* very low melt totals indicate presence of oxygen – see text for discussion

** low total due to large Pt content, as analysed by PIXE – see text for discussion

The melt analysis totals in Table 46 are very low. The surfaces of these melts appear tarnished or very badly polished, as is shown for experiment HU825 in Figures 40 and 41, but are not tarnished. Analysis by SEM confirmed that the dull grey material is Fe-oxide. As it was not possible to determine the oxygen content in the melts, it is assumed that the missing weight from the analytical totals is due to the presence of oxygen.

The low Fe total in the metal of experiment HU825 is due to a high Pt content. The large standard deviation of the Fe in the metal indicate that this phase is heterogeneous. EPMA

spot-analyses for Fe and Pt on the metal (14 points) showed that the metal consists of 8.41 wt% Pt (1σ = 1.69) and 87.02 wt% Fe (1σ = 1.73). The metal was also analysed by PIXE (Table 46), and is discussed in the following section. There is a significant difference between the Pt content determined in the metal by EPMA (8.41 wt%) and by PIXE (14.1 wt%). A beam spot with 100 µm diameter was used during PIXE analyses, while a beam spot with 1 µm diameter was used during EPMA analyses (as discussed in Section 4). During EPMA analysis spots were carefully chosen so as to exclude areas which appeared oxidised, while during PIXE analysis this was not possible, and oxidised areas were also analysed. It is possible that the Pt content in these bulk areas is higher than in the oxygen-free areas. The PIXE analyses provide a better estimation of the average PGE content in the metal phase than the EPMA analyses.

***Table 47.*** *Major element compositions, determined by EPMA, of co-existing iron and quenched melt (possibly coexisting with oxides), equilibrated at 1100°C.*

| Exp | Phase | Fe wt% (± 3σ) | S wt% (± 3σ) | Total (wt%) | PGE# (wt%) | n |
|---|---|---|---|---|---|---|
| **HU734** | Iron | 100.34 (0.27) | bd | 100.34 | ~0.2 | 18 |
| | Melt | 68.07 (0.95) | 31.66 (0.74) | *99.73 | bd | 22 |
| **HU735** | Iron | 100.15 (0.33) | bd | 100.15 | ~0.1 | 18 |
| | Melt | 65.80 (0.68) | 32.46 (0.45) | *98.26 | ~0.2 | 20 |
| **HU736** | Iron | 100.10 (0.19) | bd | 100.10 | ~0.1 | 20 |
| | Melt | 68.19 (1.12) | 31.46 (0.99) | *99.65 | ~0.1 | 26 |

# estimation of total PGE content as determined by PIXE, discussed in section 5.3.1.2.

* low melt totals indicate presence of oxygen – see text for discussion

UNIVERSITEIT VAN PRETORIA
UNIVERSITY OF PRETORIA
YUNIBESITHI YA PRETORIA

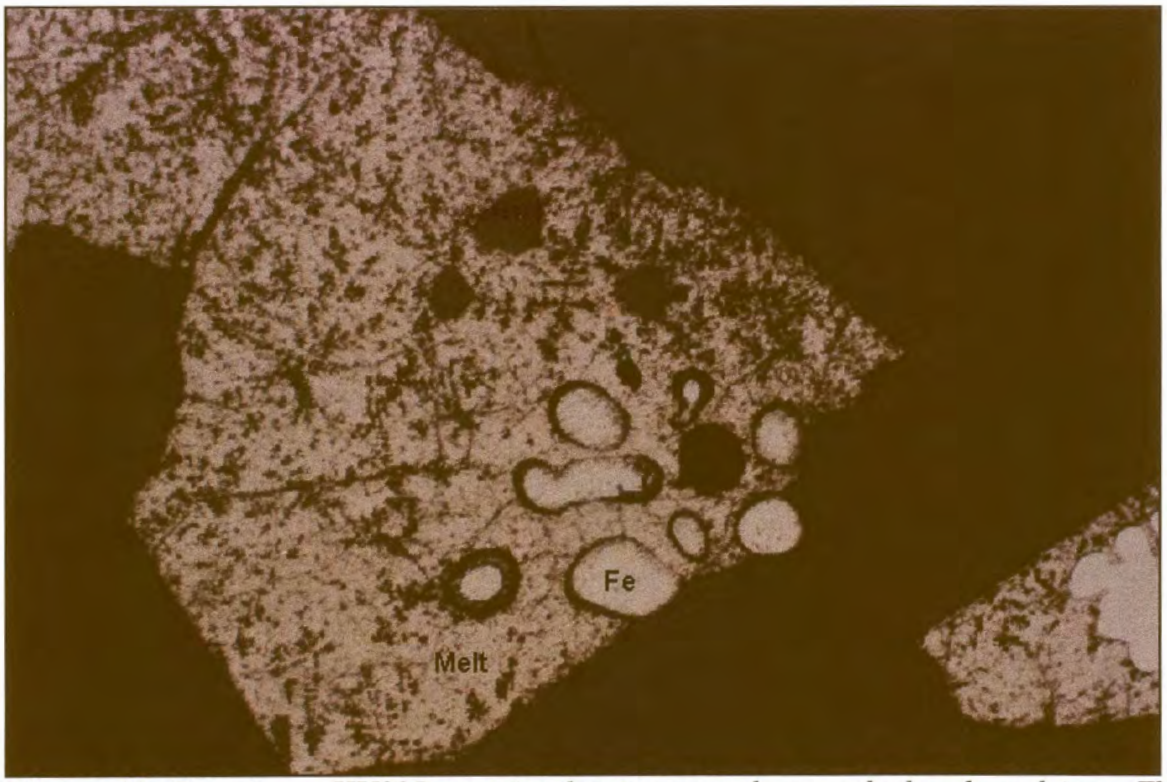


***Figure 40.*** *Experiment HU825 contains heterogeneously quenched melt and iron. The appearance of the melt is unusual. The long side of the photograph is 4 mm long.*

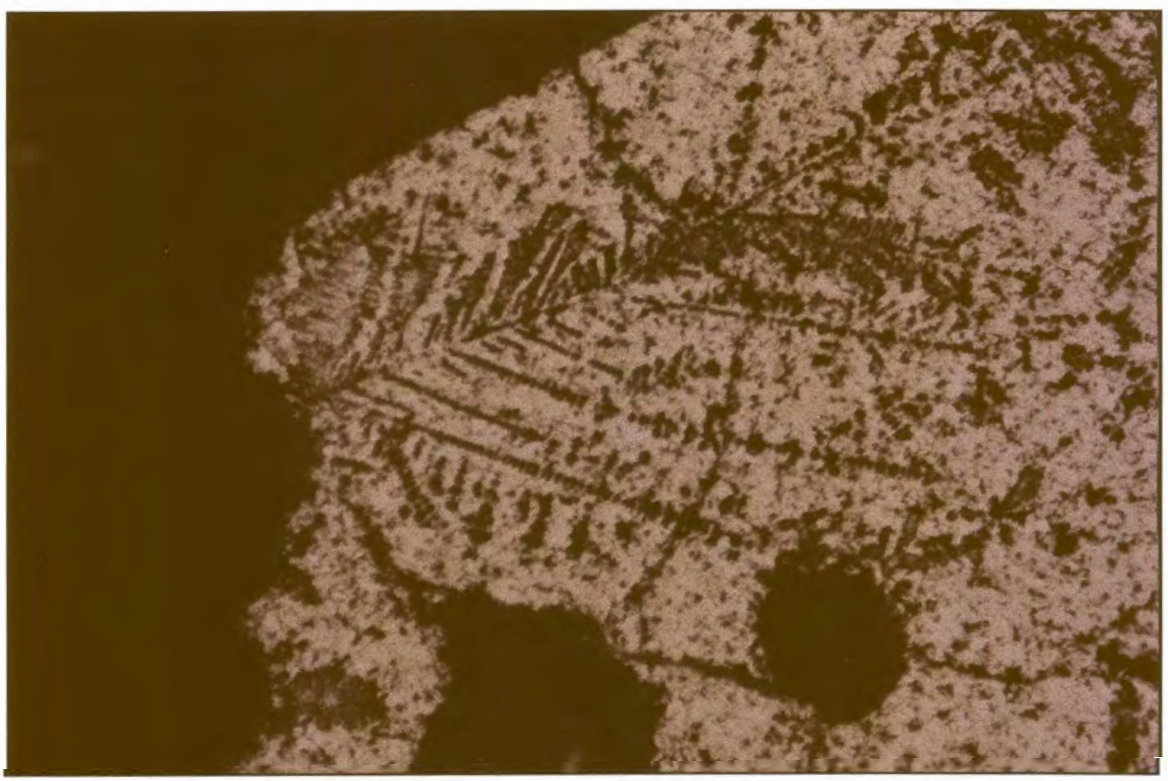

***Figure 41.*** *Enlargement of the dendrites of experiment HU825, shown in Figure 40. The dull grey dendrites were determined by electron microscopy to have high contents of Fe-oxide along with Fe. Field of view 1.4 mm.*

The melt phases of the 1100°C experiments (Table 47 - experiments HU734, HU735 and HU736) apparently contain small amounts of oxygen, but the metals appear to be free of oxygen.

All five of the experiments for which data is presented in Table 41 were exposed to oxygen to some degree. The metal phases of experiments HU843 and HU845, and especially HU844, all contain oxides as inclusions (see Figures 42, 43, 44 and 45). These were avoided during EPMA analyses, and therefore are not clearly reflected in the totals of experiments HU843 and HU845. The metal phases of experiment HU844 (Figures 44 and 45) are so diluted by oxides that it was very difficult to find positions for analysis that did not contain oxides. The low total of the metal in experiment HU844 reflects the interference from oxide. The metals of experiments HU849 and HU850 were analysed separately by EPMA for PGE. The metal of experiment HU849 was found to contain 6.30 wt% Pt ($1\sigma$ = 1.56 wt%), 3.82 wt% Rh ($1\sigma$ = 0.59 wt%) and no detectable Pd. During PIXE analysis, the oxides in the metal could not be avoided, and much lower PGE contents were determined. The Pt and Rh could be more concentrated in the oxide-free areas of the metal. The metal of experiment HU850 contains about 0.13 wt% Pt ($1\sigma$ = 0.06 wt%), 1.11 wt% Rh ($1\sigma$ = 0.09 wt%) and no detectable Pd. Apparently the oxygen formed separate Fe oxides in the metal phase, but it is unclear whether Fe oxides were formed in the melt, or if the oxygen was incorporated into the structure of the sulphide melt.

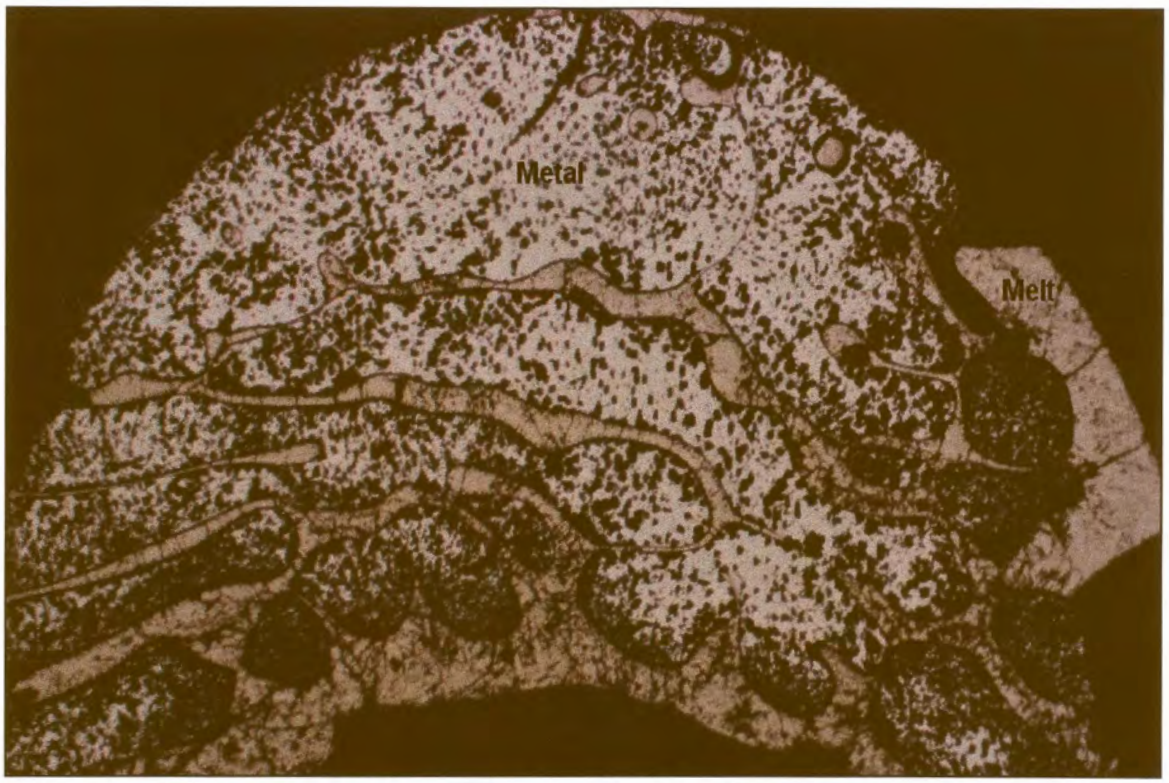


***Figure 42.*** *Experiment HU845 contains metal and melt that were equilibrated at 1000°C. Both phases contain Fe oxides (grey inclusions). Field of view 4 mm.*

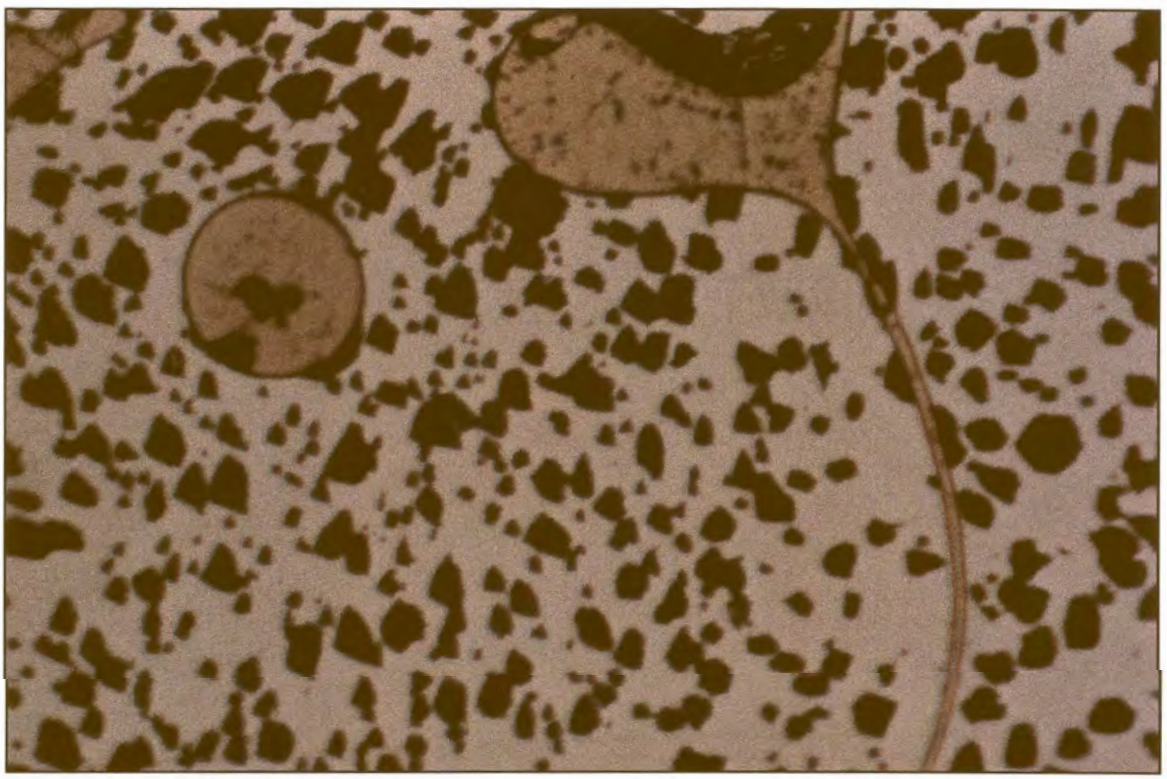

***Figure 43.*** *Enlargement of the metal and melt phases of experiment HU845 shown in Figure 42. The grey oxides are scattered through the metal. Field of view 0.6 mm.*

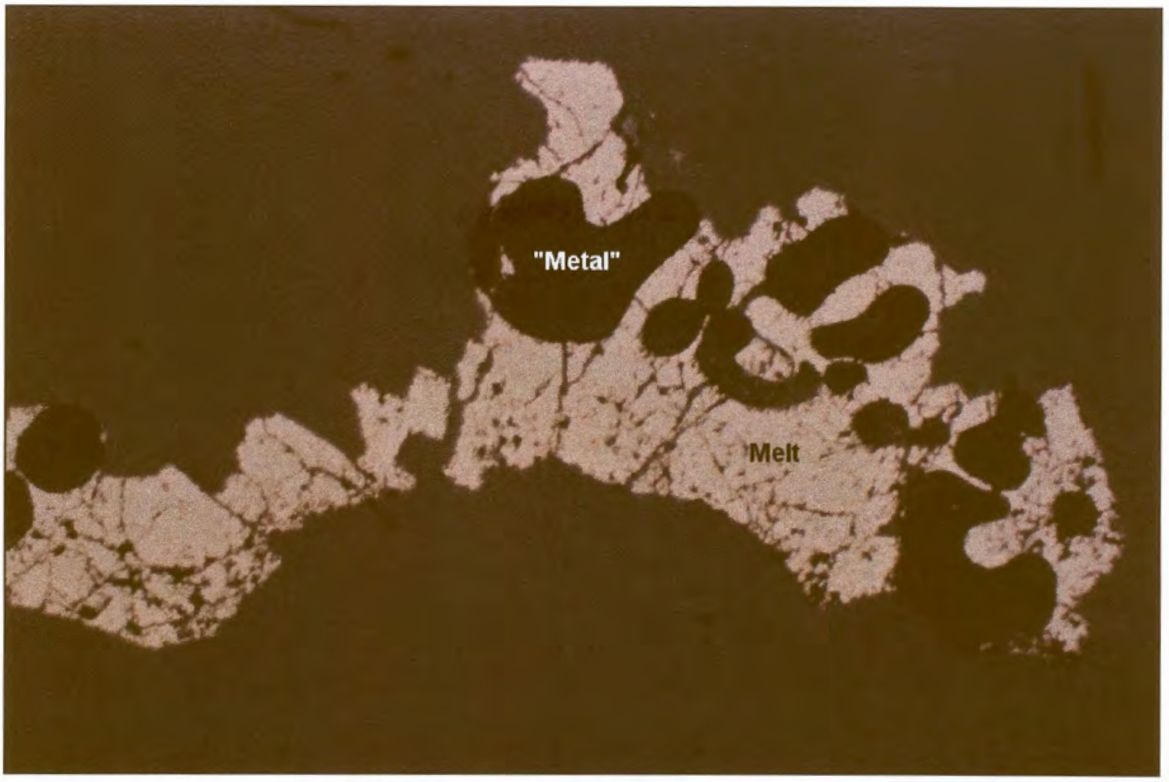


***Figure 44.*** *Experiment HU844 should have contained metal and melt that were equilibrated at 1000°C. The "metal" phase is unrecognisable due to the low reflectivity oxides scattered all through it. Field of view 4 mm.*

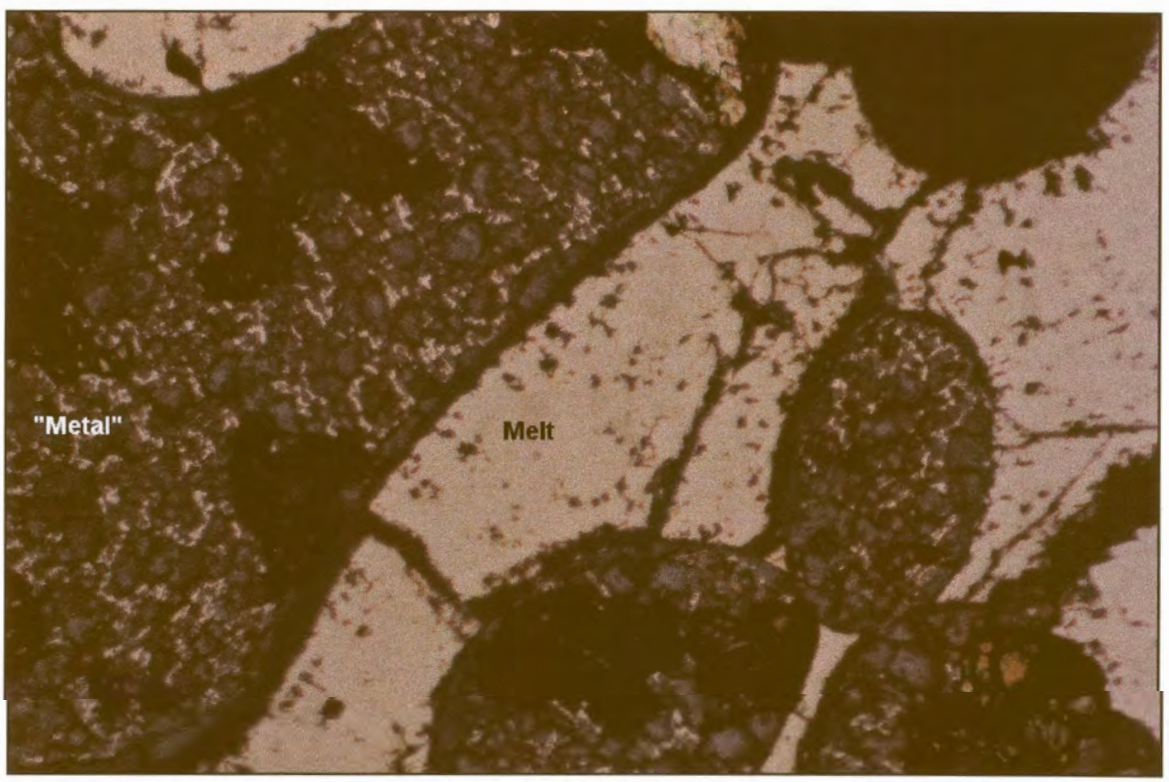


***Figure 45.*** *Higher magnification of the "metal" phase of experiment HU844, in Figure 44. Large Fe-oxide crystals imply late stage oxidation. Field of view 0.6 mm.*

***Table 48.*** *Major element compositions, determined by EPMA, of co-existing iron and quenched melt equilibrated at 1000°C. Some of the metal contains oxides, and some of the sulphide melts oxygen, which influenced the analyses.*

| Exp | Phase | Fe wt% (± 3σ) | S wt% (± 3σ) | Total (wt%) | PGE# (wt%) | n |
|---|---|---|---|---|---|---|
| **HU843** | Iron | 99.72 (0.32) | bd | 99.72 | ~0.4 | 20 |
| | Melt | 63.09 (0.70) | 35.42 (0.83) | *98.51 | ~0.3 | 20 |
| **HU844** | Iron | 60.47 (5.97) | 1.71 (0.64) | *62.18 | ~0.1 | 30 |
| | Melt | 63.08 (0.56) | 34.19 (1.01) | *97.27 | <0.06 | 48 |
| **HU845** | Iron | 99.47 (0.34) | bd | 99.47 | ~0.3 | 20 |
| | Melt | 62.81 (0.38) | 34.05 (1.09) | *96.86 | ~0.1 | 40 |
| **HU849** | Iron | 89.29 (1.64) | bd | *89.29 | ~0.1 | 20 |
| | Melt | 63.90 (0.34) | 33.50 (0.64) | *97.40 | <0.1 | 25 |
| **HU850** | Iron | 97.78 (0.53) | bd | *97.78 | ~1.2 | 26 |
| | Melt | 65.23 (1.01) | 33.00 (1.46) | *98.23 | ~0.3 | 26 |

\# estimation of total PGE content as determined by PIXE, discussed in section 5.3.1.2.

* low totals indicate presence of oxygen – see text for discussion

The compositions of all the experiments that contained the iron – melt assemblage were projected onto the Fe-S phase diagram (after Chuang *et al.*, 1985), ignoring the presence of oxygen and PGE (Figure 24 – blue triangles). From this projection it is clear that the experiments cannot be projected onto the binary phase diagram and contain significant amounts of at least one additional element.

### 5.3.1.2. PIXE results

#### 5.3.1.2.1. Milli-PIXE

##### 5.3.1.2.1.1. Results for equilibration at 1200°C

Two analyses were performed on the "iron" of experiment HU825, and the average as determined with resampling was used in further discussion (Table 55). The second analysis of the iron of experiment HU826 was used.

***Table 49.*** *Milli-PIXE trace element analyses of the metal that co-exists with melt in the Fe – S ± O system, equilibrated at 1200°C.*

| Exp | Rh wt% (± 3σ) | Rh LLD | Pd wt% (± 3σ) | Pd LLD | Pt wt% (± 3σ) | Pt LLD | Counts |
|---|---|---|---|---|---|---|---|
| **HU825** | | | | | 13.49 (0.19) | 0.12 | 500000 |
| **HU825** | | | | | 14.70 (0.24) | 0.12 | 500000 |
| **HU826** | | | bd | 0.20 | | | 500000 |
| **HU826** | | | 0.22 (0.07) | 0.10 | | | 500000 |
| **HU827** | 0.47 (0.09) | 0.10 | | | | | 500000 |

Pt was detected in the second analysis of the melt of experiment HU825. The average Pd content as determined with resampling statistics from two analyses performed on the melt of experiment HU826 was used, and similarly the average Rh content of the two analyses on the melt of experiment HU827 (Table 55).

***Table 50.*** *Milli-PIXE trace element analyses of the melt that co-exists with metal in the Fe – S ±O system, equilibrated at 1200°C.*

| Exp | Rh wt% (± 3σ) | Rh LLD | Pd wt% (± 3σ) | Pd LLD | Pt wt% (± 3σ) | Pt LLD | Counts |
|---|---|---|---|---|---|---|---|
| **HU825** | | | | | *0.04* (0.03) | 0.05 | 500000 |
| **HU825** | | | | | 0.06 (0.03) | 0.05 | 500000 |
| **HU826** | | | 0.21(0.05) | 0.06 | | | 500000 |
| **HU826** | | | 0.28 (0.07) | 0.10 | | | 500000 |
| **HU827** | 0.09 (0.05) | 0.07 | | | | | 500000 |
| **HU827** | 0.14 (0.06) | 0.10 | | | | | 500000 |

**5.3.1.2.1.2.** Results for equilibration at 1100°C

In both analyses of the metal of experiment HU734 Pt was below detection, and the lowest detection limit was used. The Pd content of the first analysis on the metal of experiment HU735 was below detection, and the second analysis was used.

***Table 51.*** *Milli-PIXE trace element analyses of the metal that co-exists with melt in the Fe – S ± O system, equilibrated at 1100°C.*

| Exp | Rh wt% (± 3σ) | Rh LLD | Pd wt% (± 3σ) | Pd LLD | Pt wt% (± 3σ) | Pt LLD | Counts |
|---|---|---|---|---|---|---|---|
| **HU734** | | | | | bd | 0.15 | 500000 |
| **HU734** | | | | | bd | 0.30 | 500000 |
| **HU735** | | | *0.04* (0.05) | 0.09 | | | 500000 |
| **HU735** | | | 0.16 (0.06) | 0.11 | | | 500000 |
| **HU736** | 0.12 (0.05) | 0.08 | | | | | 500000 |

The Pt content in the melt of experiment HU734 was below the detection limit. The first analysis on the melt of experiment HU736 could not detect any Rh and therefore the second analysis is used (Table 55).

***Table 52.*** *Milli-PIXE trace element analyses of the melt that co-exists with metal in the Fe - S ± O system, equilibrated at 1100°C.*

| Exp | Rh wt% (± 3σ) | Rh LLD | Pd wt% (± 3σ) | Pd LLD | Pt wt% (± 3σ) | Pt LLD | Counts |
|---|---|---|---|---|---|---|---|
| **HU734** | | | | | 0.04 (0.03) | 0.05 | 500000 |
| **HU735** | | | 0.21 (0.07) | 0.12 | | | 500000 |
| **HU736** | 0.05 (0.04) | 0.07 | | | | | 500000 |
| **HU736** | 0.13 (0.06) | 0.10 | | | | | 500000 |

**5.3.1.2.1.3.** Results for equilibration at 1000°C

The average Pd content of the two analyses on the metal of experiment HU843, and the average Rh content of two analyses on the metal of experiment HU844, were determined with resampling statistics. The average Rh content and the average Pd content of the two analyses on the metal of experiment HU845 were determined with resampling statistics, and the lowest detection limit for Pt was used. Of the three analyses performed on the metal of experiment HU849, the average Rh content of the first two was determined with resampling statistics, the lowest Pd detection limit was used, and the Pt content in the second analysis

was used. For the melt of experiment HU850, the average Rh and Pd contents were determined. The average of the Pt analyses was also determined, although the first analysis is statistically unreliable. Values used for further calculations are provided in Table 55.

***Table 53**. Milli-PIXE trace element analyses of the metal that co-exists with melt in the Fe-S (±O) system, equilibrated at 1000°C.*

| Exp | Rh wt% (± 3σ) | Rh LLD | Pd wt% (± 3σ) | Pd LLD | Pt wt% (± 3σ) | Pt LLD | Counts |
|---|---|---|---|---|---|---|---|
| **HU843** | | | 0.57 (0.10) | 0.07 | | | 500000 |
| **HU843** | | | 0.30 (0.07) | 0.09 | | | 500000 |
| **HU844** | 0.13 (0.05) | 0.07 | | | | | 500000 |
| **HU844** | 0.10 (0.03) | 0.03 | | | | | 500000 |
| **HU845** | 0.21 (0.05) | 0.06 | 0.10 (0.04) | 0.06 | *0.02* (0.04) | 0.07 | 500000 |
| **HU845** | 0.17 (0.05) | 0.07 | 0.19 (0.06) | 0.10 | *0.02* (0.04) | 0.08 | 500000 |
| **HU849** | 0.09 (0.02) | 0.02 | *0.01* (0.02) | 0.04 | *0.06* (0.04) | 0.08 | 500000 |
| **HU849** | 0.13 (0.04) | 0.05 | *0.06* (0.04) | 0.07 | 0.09 (0.04) | 0.07 | 500000 |
| **HU849** | bd | 0.16 | bd | 0.10 | *0.06* (0.05) | 0.08 | 500000 |
| **HU850** | 0.73 (0.09) | 0.11 | 0.53 (0.09) | 0.14 | *0.08* (0.05) | 0.08 | 500000 |
| **HU850** | 0.84 (0.12) | 0.13 | 0.21 (0.09) | 0.14 | 0.14 (0.06) | 0.09 | 500000 |

The Pd content of the two analyses on the melt of experiment HU843 was averaged. In all three of the analyses on the melt of experiment HU844, Rh was below detection. All PGE were below detection in the melt of experiment HU845. Similarly, no PGE could be detected during the two analyses on the melt of experiment HU849. Of the two analyses on the melt of experiment HU850, the values for Rh and Pd from the second analysis was used. Pt was only observed above the detection limit in the first analysis, and this value will be used.

***Table 54***. *Milli-PIXE trace element analyses of the melt that co-exists with metal in the Fe-S (±O) system, equilibrated at 1000°C.*

| Exp | Rh wt% (± 3σ) | Rh LLD | Pd wt% (± 3σ) | Pd LLD | Pt wt% (± 3σ) | Pt LLD | Counts |
|---|---|---|---|---|---|---|---|
| **HU843** | | | 0.22 (0.07) | 0.07 | | | 500000 |
| **HU843** | | | 0.31(0.09) | 0.10 | | | 500000 |
| **HU844** | *0.02* (0.03) | 0.06 | | | | | 500000 |
| **HU844** | *0.03* (0.04) | 0.07 | | | | | 500000 |
| **HU844** | bd | 0.07 | | | | | 500000 |
| **HU845** | bd | 0.12 | *0.07* (0.07) | 0.13 | *0.03* (0.04) | 0.07 | 500000 |
| **HU845** | bd | 0.09 | *0.09* (0.07) | 0.13 | *0.03* (0.03) | 0.05 | 500000 |
| **HU849** | *0.04* (0.03) | 0.05 | bd | 0.13 | bd | 0.08 | 500000 |
| **HU849** | bd | 0.12 | *0.08* (0.07) | 0.12 | bd | 0.08 | 500000 |
| **HU850** | bd | 0.13 | 0.14 (0.07) | 0.10 | 0.08 (0.03) | 0.05 | 500000 |
| **HU850** | 0.12 (0.05) | 0.06 | 0.24 (0.08) | 0.13 | *0.04* (0.04) | 0.06 | 500000 |

***Table 55***. *Results of milli-PIXE analyses of the iron - sulphide melt assemblage in experiments of the Fe - S system.*

| Exp | Temp (°C) | Iron | | | Sulphide melt | | |
|---|---|---|---|---|---|---|---|
| | | Rh (wt%) | Pd (wt%) | Pt (wt%) | Rh (wt%) | Pd (wt%) | Pt (wt%) |
| **HU825** | 1200 | | | 14.10 | | | 0.06 |
| **HU826** | 1200 | | 0.22 | | | 0.25 | |
| **HU827** | 1200 | 0.47 | | | 0.11 | | |
| **HU734** | 1100 | | | <0.15 | | | <0.05 |
| **HU735** | 1100 | | 0.16 | | | 0.21 | |
| **HU736** | 1100 | 0.12 | | | 0.13 | | |
| **HU843** | 1000 | | 0.44 | | | 0.27 | |
| **HU844** | 1000 | 0.12 | | | <0.06 | | |
| **HU845** | 1000 | 0.19 | 0.15 | <0.07 | <0.09 | <0.13 | <0.05 |
| **HU849** | 1000 | 0.11 | <0.04 | 0.09 | <0.05 | <0.12 | <0.08 |
| **HU850** | 1000 | 0.78 | 0.37 | 0.11 | 0.12 | 0.24 | 0.08 |

### 5.3.2. Pyrrhotite – Fe-S melt assemblage (1100°C)

#### 5.3.2.1. EPMA results

The major element compositions of the co-existing pyrrhotite and melt in the experiments equilibrated at 1100°C, determined by EPMA, are given in Table 56. These compositions are also indicated on the Fe-S phase diagram (Figure 24 – green triangles). The compositions of the melt and pyrrhotite determined by EPMA do not plot at opposite sides of the original bulk experimental composition (Figure 24). This indicates that at least one more element influences the major elemnt compositions, possibly oxygen, even though the material does not look oxidised, and the totals from the EPMA analyses approach 100 %.

***Table 56.*** *Major element compositions, determined by EPMA, of co-existing pyrrhotite and quenched melt equilibrated at 1100°C.*

| Exp | Phase | Fe wt% (± 3σ) | S wt% (± 3σ) | Total (wt%) | PGE# (wt%) | n |
|---|---|---|---|---|---|---|
| **HU737** | Melt | 64.06 (0.34) | 35.38 (0.41) | 99.44 | ~0.2 | 14 |
| | Pyrrhotite | 62.87 (0.11) | 37.77 (0.12) | 100.64 | <0.04 | 18 |
| **HU738** | Melt | 63.95 (0.38) | 34.81 (0.25) | 98.76 | ~0.2 | 30 |
| | Pyrrhotite | 62.79 (0.11) | 37.65 (0.17) | 100.44 | <0.02 | 20 |
| **HU739** | Melt | 64.54 (0.34) | 35.33 (0.41) | 99.87 | ~0.1 | 22 |
| | Pyrrhotite | 62.69 (0.13) | 37.26 (0.18) | 99.95 | <0.03 | 19 |

# estimation of total PGE content as determined by PIXE, discussed in section 5.3.2.2.

#### 5.3.2.2. PIXE results

##### 5.3.2.2.1. Milli-PIXE

Two analyses were performed on each of the melt phases, and the averages were determined with resampling statistics. Pt was below detection for both analyses of the pyrrhotite of experiment HU737 (Table 58), Pd was below detection in both analyses of the

pyrrhotite of experiment HU738, and the Rh content in both analyses of the pyrrhotite of experiment HU739 was below detection limits.

***Table 57.*** *Milli-PIXE trace element analyses of the melt that co-exists with pyrrhotite in the Fe-S system, equilibrated at 1100°C.*

| Exp | Rh wt% (± 3σ) | Rh LLD | Pd wt% (± 3σ) | Pd LLD | Pt wt% (± 3σ) | Pt LLD | Counts |
|---|---|---|---|---|---|---|---|
| **HU737** | | | | | 0.14 (0.02) | 0.03 | 500000 |
| **HU737** | | | | | 0.15 (0.02) | 0.03 | 500000 |
| **HU738** | | | 0.21 (0.03) | 0.03 | | | 500000 |
| **HU738** | | | 0.21 (0.03) | 0.03 | | | 500000 |
| **HU739** | 0.13 (0.03) | 0.04 | | | | | 500000 |
| **HU739** | 0.09 (0.02) | 0.03 | | | | | 500000 |

***Table 58.*** *Milli-PIXE trace element analyses of the pyrrhotite that co-exists with melt in the Fe-S system, equilibrated at 1100°C.*

| Exp | Rh wt% (± 3σ) | Rh LLD | Pd wt% (± 3σ) | Pd LLD | Pt wt% (± 3σ) | Pt LLD | Counts |
|---|---|---|---|---|---|---|---|
| **HU737** | | | | | 0.02 (0.02) | 0.04 | 500000 |
| **HU737** | | | | | bd | 0.04 | 500000 |
| **HU738** | | | 0.02 (0.02) | 0.03 | | | 500000 |
| **HU738** | | | 0.01 (0.01) | 0.02 | | | 500000 |
| **HU739** | 0.01 (0.01) | 0.03 | | | | | 500000 |
| **HU739** | 0.01 (0.02) | 0.03 | | | | | 500000 |

***Table 59.*** *Results of milli-PIXE analyses of the melt-pyrrhotite assemblage in experiments of the Fe-S system.*

| Exp | Temp (°C) | Melt | | | Pyrrhotite | | |
|---|---|---|---|---|---|---|---|
| | | Rh (wt%) | Pd (wt%) | Pt (wt%) | Rh (wt%) | Pd (wt%) | Pt (wt%) |
| **HU737** | 1100 | | | 0.15 | | | <0.04 |
| **HU738** | 1100 | | 0.21 | | | <0.02 | |
| **HU739** | 1100 | 0.11 | | | <0.03 | | |

### 5.3.3. Iron - troilite assemblage (900°C)

#### 5.3.3.1. EPMA results

The major element compositions of co-existing iron and troilite in experiments equilibrated at 900°C, determined by EPMA, are given in Table 60. The compositions are also shown on the phase diagram of the Fe-S system (Figure 24 – pink triangles). There is no evidence that these experiments were contaminated by oxygen.

***Table 60.*** *Major element compositions, determined by EPMA, of co-existing iron and troilite equilibrated at 900°C.*

| Exp | Phase | Fe wt% (± 3σ) | S wt% (± 3σ) | Total (wt%) | PGE# (wt%) | n |
|---|---|---|---|---|---|---|
| **HU434** | Iron | 99.53 (0.44) | - | 99.53 | ~0.1 | 26 |
| | Troilite | 63.03 (0.45) | 37.09 (0.20) | 100.12 | <0.05 | 30 |
| **HU435** | Iron | 99.89 (0.52) | - | 99.89 | <0.28 | 25 |
| | Troilite | 62.84 (0.25) | 36.74 (0.33) | 99.58 | <0.89 | 28 |
| **HU436** | Iron | 99.60 (0.66) | - | 99.60 | ~0.2 | 28 |
| | Troilite | 62.62 (0.37) | 37.11 (0.30) | 99.73 | <0.08 | 28 |
| **HU756** | Iron | 100.50 (0.27) | - | 100.50 | ~0.3 | 30 |
| | Troilite | 63.10 (0.17) | 37.07 (0.17) | 100.17 | ~0.1 | 30 |

# Estimation of total PGE content as determined by PIXE, discussed in section 5.3.3.2.

#### 5.3.3.2. PIXE results

##### 5.3.3.2.1. Milli-PIXE

###### 5.3.3.2.1.1. Results for equilibration at 900°C

In the three analyses of the iron of experiment HU756, Rh was detected in the first two, and the average as determined with resampling statistics was used. Pd could also be detected in two of the analyses, and although the two results vary a lot, the average determined with

resampling statistics was used. The detection limit for Pt was low enough in only the last analysis to allow observation of Pt.

***Table 61.*** *Milli-PIXE trace element analyses of iron that co-exists with troilite in the Fe-S system, equilibrated at 900°C.*

| Exp | Rh wt% (± 3σ) | Rh LLD | Pd wt% (± 3σ) | Pd LLD | Pt wt% (± 3σ) | Pt LLD | Counts |
|---|---|---|---|---|---|---|---|
| **HU434** | | | | | bd | 0.09 | 500000 |
| **HU434** | | | | | 0.14 (0.04) | 0.06 | 500000 |
| **HU435** | | | bd | 0.28 | | | 500000 |
| **HU435** | | | bd | 1.54 | | | 500000 |
| **HU436** | 0.17 (0.06) | 0.11 | | | | | 500000 |
| **HU436** | *0.02* (0.05) | 0.10 | | | | | 500000 |
| **HU756** | 0.13 (0.04) | 0.06 | *0.05* (0.04) | 0.08 | *0.05* (0.05) | 0.08 | 500000 |
| **HU756** | 0.14 (0.04) | 0.06 | 0.21 (0.06) | 0.11 | *0.01* (0.05) | 0.09 | 500000 |
| **HU756** | bd | 0.07 | 0.10 (0.04) | 0.04 | 0.08 (0.02) | 0.04 | 500000 |

***Table 62.*** *Milli-PIXE trace element analyses of the troilite that co-exists with metal in the Fe-S system, equilibrated at 900°C.*

| Exp | Rh wt% (± 3σ) | Rh LLD | Pd wt% (± 3σ) | Pd LLD | Pt wt% (± 3σ) | Pt LLD | Counts |
|---|---|---|---|---|---|---|---|
| **HU434** | | | | | bd | 0.05 | 500000 |
| **HU434** | | | | | bd | 0.05 | 500000 |
| **HU435** | | | 0.72 (0.53) | 0.89 | | | 500000 |
| **HU435** | | | 1.95 (1.34) | 2.27 | | | 500000 |
| **HU436** | bd | 0.08 | | | | | 500000 |
| **HU436** | bd | 0.10 | | | | | 500000 |
| **HU756** | bd | 0.04 | 0.04 (0.04) | 0.07 | bd | 0.05 | 500000 |
| **HU756** | bd | 0.04 | 0.14 (0.03) | 0.04 | bd | 0.05 | 500000 |

No Pt was detected in the two analyses of the troilite of experiment HU434 (Table 62), and the detection limit was used. The detection limits during both analyses of the troilite of

experiment HU435 were very high, and no Pd could be detected. The lowest Rh detection limit from the two analyses of the troilite of experiment HU436 was used. Two analyses were performed of the troilite of experiment HU756, and in both cases Rh was below detection limits. Pd was detected in the second analysis, but Pt could not be detected in either analyses. Values used in further calculations are shown in Table 63.

***Table 63.*** *Results of milli-PIXE analyses of the iron-troilite assemblage in experiments of the Fe-S system.*

| Exp | Temp | Iron | | | Troilite | | |
|---|---|---|---|---|---|---|---|
| | (°C) | Rh (wt%) | Pd (wt%) | Pt (wt%) | Rh (wt%) | Pd (wt%) | Pt (wt%) |
| **HU434** | 900 | | | 0.14 | | | <0.05 |
| **HU435** | 900 | | <0.28 | | | <0.89 | |
| **HU436** | 900 | 0.17 | | | <0.08 | | |
| **HU756** | 900 | 0.14 | 0.16 | 0.08 | <0.04 | 0.14 | <0.05 |

# 6. Discussion

It is obvious from the information obtained from EPMA, milli-PIXE, and micro-PIXE analyses (Section 5) that different analytical methods and different instruments show different concentrations for the same element in a phase. This problem was addressed by Franklyn and Merkle (1999) and Merkle *et al.* (in print). However, if the same element is successively analysed in two co-existing phases utilising the same instrument, and the ratio of these results is calculated, the instrumental influence on these results should be cancelled out or limited. In the present investigation, the partitioning of the three PGE Rh, Pd and Pt is examined between phases in the three systems Ni-S, Cu-S and Fe-S(±O), using Nernst partition coefficients (D).

## 6.1. The Ni-S system

### 6.1.1. Nickel – Ni-S melt assemblage (1100°C - 700°C)

Nernst partition coefficient: D = (PGE content in metal) / (PGE content in melt).

D were calculated from the micro-PIXE and milli-PIXE analyses discussed in section 5.1.1.2. (Tables 20 and 27). The ratios were obtained with resampling statistics (as discussed in section 4.3.), which made it possible to determine confidence intervals for the ratios. Tables 64 and 65 contain the D calculated separately for milli-PIXE and micro-PIXE results. These values vary a lot for the three elements between the two Tables (or two PIXE instruments), and also vary according to equilibration temperatures, PGE contents, and possibly the presence or absence of other PGE in the systems. The influence of these factors on the partition coefficients will be discussed below.

***Table 64.*** *D (metal/melt) for the PGE determined for Ni metal and melt assemblages from the milli-PIXE results in Table 20.*

| Exp | Temp (°C) | PGE (ppm) | $D_{Rh}$ (± 1σ) | $D_{Pd}$ (± 1σ) | $D_{Pt}$ (± 1σ) |
|---|---|---|---|---|---|
| **HU733** | 1100 | 500 | 1.6 (0.3) | 0.5 (0.1) | 4.1 (0.7) |
| **HU731** | 1100 | 2000 | | | 4.8 (0.8) |
| **HU393** | 1000 | 1000 | 2.8 (0.1) | 0.6 (0.04) | 23.2 (5.5) |
| **HU381** | 1000 | 2000 | 4.0 (0.5) | 0.7 (0.1) | 26.7 (4.5) |
| **HU753** | 900 | 1000 | 4.2 (0.5) | 0.8 (0.1) | >14.4 |
| **HU429** | 900 | 2000 | 5.5 (0.3) | 0.6 (0.03) | >26.8 |
| **HU427** | 900 | 2000 | | 0.9 (0.03) | |
| **HU469** | 700 | 500 | 5.5 (0.5) | 0.5 (0.1) | >4.9 |
| **HU471** | 700 | 2000 | | | >25.8 |
| **HU473** | 700 | 2000 | 9.9 (1.5) | | |

***Table 65.*** *D (metal/melt) for the PGE determined for Ni metal and melt assemblages from the micro-PIXE results in Table 27.*

| Exp | Temp (°C) | PGE (ppm) | $D_{Rh}$ (± 1σ) | $D_{Pd}$ (± 1σ) | $D_{Pt}$ (± 1σ) |
|---|---|---|---|---|---|
| **HU441** | 1100 | 2000 | 2.7 (0.1) | 0.5 (0.02) | 19.9 (1.0) |
| **HU437** | 1100 | 2000 | | 0.7 (0.03) | |
| **HU393** | 1000 | 1000 | 4.7 (0.1) | 0.8 (0.03) | 49.3 (3.4) |
| **HU394** | 1000 | 6000 | 4.4 (0.07) | 0.6 (0.01) | 45.6 (2.4) |
| **HU395** | 1000 | 10000 | 3.9 (0.05) | 0.6 (0.01) | 56.2 (1.0) |
| **HU412** | 1000 | 10000 | 3.8 (0.1) | 0.7 (0.01) | 44.7 (1.3) |
| **HU392** | 1000 | ? | 7.1 (0.1) | 0.9 (0.1) | 219 (29) |
| **HU429** | 900 | 2000 | 5.3 (0.1) | 0.7 (0.01) | 84 (8) |
| **HU426** | 900 | 2000 | | | 97 (34) |
| **HU427** | 900 | 2000 | | 0.7 (0.02) | |
| **HU428** | 900 | 2000 | 5.4 (0.1) | | |

? = discussed in text, section 5.1.1.1. (separated drop with unplanned composition)

#### 6.1.1.1. Variation of partition coefficients with different instruments

Only experiments HU393, HU427 and HU429 were investigated by both micro- and milli-PIXE, and can be used to compare results from the two instruments. For experiment HU393 $D_{Rh}$ (4.7) and $D_{Pt}$ (49.1) from micro-PIXE analyses are almost twice those from milli-PIXE analyses: $D_{Rh}$ (2.8) and $D_{Pt}$ (22.6). $D_{Pd}$ varies from 0.8 from micro-PIXE to 0.6 from milli-PIXE analyses. This might imply higher sensitivity of the milli-PIXE for PGE in the metal phase, or lower PGE sensitivity in the melt phase. The partition coefficients for experiment HU429 compare better. $D_{Rh}$ varies from 5.5 to 5.3 and $D_{Pd}$ from 0.6 to 0.7. The micro-PIXE value for $D_{Pt}$ is 84 (Table 65), while the milli-PIXE value (Table 64) is > 26.8. The $D_{Pd}$ values for experiment HU427 are 0.7 and 0.9 respectively.

In order to get a clearer indication of the difference in sensitivities between the instruments, the determined PGE contents for the separate phases are shown in Table 66, where the results from milli- and micro-PIXE can be compared directly. The PGE content determined for each phase by milli-PIXE was plotted against the PGE content determined for the same phase by micro-PIXE (Figure 46). From Figure 46 it becomes apparent that at higher concentrations analysed, Pd is over-represented by the milli-PIXE analyses compared to the micro-PIXE analyses, which is not the case at lower Pd concentrations. As a result, the Pd ratio, which was determined in this system by dividing the lower concentration by the higher concentration, would be somewhat lower for milli-PIXE – as was seen to be the case. Pt, on the other hand, is slightly over-represented in the micro-PIXE analysis. When the higher Pt ratio is determined by dividing the higher concentration by the lower concentration, a too-high ratio will be obtained, as was observed in the present situation.

***Table 66.*** *PGE contents in nickel and sulphide melt determined by both milli- and micro-PIXE.*

| Exp | | Milli-PIXE | | | Micro-PIXE | | |
|---|---|---|---|---|---|---|---|
| | | Rh wt% (± 3σ) | Pd wt% (± 3σ) | Pt wt% (± 3σ) | Rh wt% (± 3σ) | Pd wt% (± 3σ) | Pt wt% (± 3σ) |
| **HU393** | Nickel | 0.391(0.024) | 0.111(0.020) | 0.555(0.026) | 0.349(0.014) | 0.096(0.013) | 0.737(0.025) |
| | Melt | 0.141(0.014) | 0.184(0.017) | 0.025(0.015) | 0.075(0.002) | 0.124(0.003) | 0.015(0.001) |
| **HU427** | Nickel | | 0.304(0.023) | | | 0.159(0.008) | |
| | Melt | | 0.352(0.026) | | | 0.215(0.008) | |
| **HU429** | Nickel | 0.737(0.032) | 0.219(0.023) | 0.778(0.029) | 0.606(0.020) | 0.151(0.009) | 0.919(0.020) |
| | Melt | 0.134(0.017) | 0.344(0.024) | *0.006*(0.016) | 0.115(0.004) | 0.225(0.004) | 0.011(0.002) |

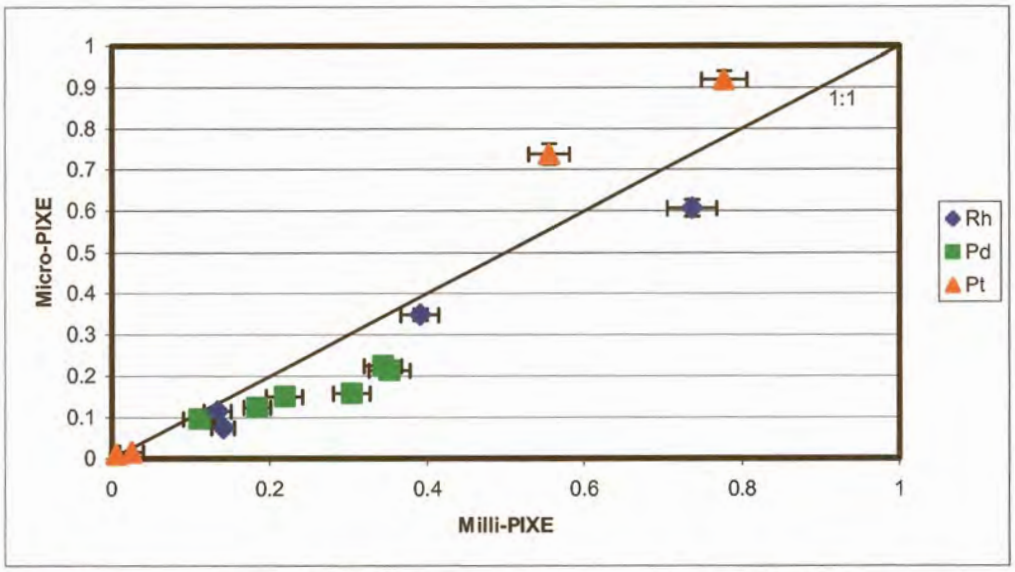


***Figure 46.*** *Comparison of PGE contents determined by milli-PIXE and micro-PIXE in corresponding phases from experiments HU393, HU427 and HU429. Error bars show 3σ standard deviations.*

An alternative explanation could be the influence of the two different software packages (GUPIX and GEOPIXE) used to analyse the spectra from the two instruments, and the deviations in D could be software-related. In a recent study of Pt-Pd-Ni-S phases (Merkle *et al.*, in print), EPMA results and milli-PIXE results using GUPIX were comparable. However, the results from GEOPIXE analyses of the spectra differed significantly (R. Merkle, personal communications). The effect of different software packages used to

interpret spectra would probably vary with the composition of the matrix analysed, but requires further evaluation. As a result of these observations, the Milli-PIXE (GUPIX) results are preferred to the micro-PIXE (GEOPIXE) results.

The differences in results between the two instruments suggest that the determination of partition coefficients is influenced by many factors and that results from different instruments cannot be directly compared. The magnitude of the fractionation of a PGE into a specific phase in an assemblage remains within the same order of magnitude for both instruments.

#### 6.1.1.2. Variation of partition coefficients with equilibration temperature

D tends to decrease with increasing temperature. Figure 47 shows the milli-PIXE D (from Table 64) of experiments HU733 and HU469, plotted against equilibration temperature. Both experiments contained 500 ppm of each of Rh, Pd and Pt. $D_{Rh}$ decreases very clearly, $D_{Pd}$ remains constant, and $D_{Pt}$ at 700°C is a minimum value, higher than $D_{Pt}$ at 1100°C.

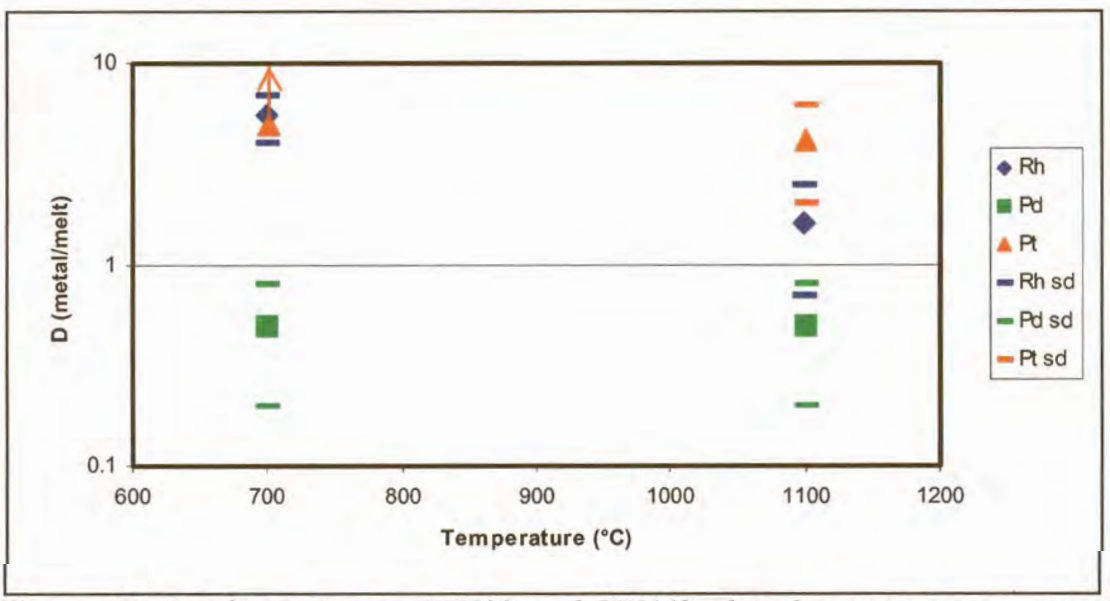


***Figure 47.*** *D of experiments HU733 and HU469 plotted against temperature. Both experiments contained 500 ppm of each PGE. $D_{Pt}$ at 700°C (HU469) is a minimum value (arrow indicates possible higher values). Error bars show 3σ standard deviations.*

Figure 48 shows the D of experiments HU381 and HU429 plotted against equilibration temperature (from Table 64). Both experiments contained 2000 ppm of each PGE. The decrease of $D_{Rh}$ over the 100°C temperature increase is clear. The apparent increase of $D_{Pd}$ from 900°C to 1000°C is not significant, considering the associated errors. $D_{Pt}$ at 900°C is a minimum value, but suggests a decrease in the partition coefficient.

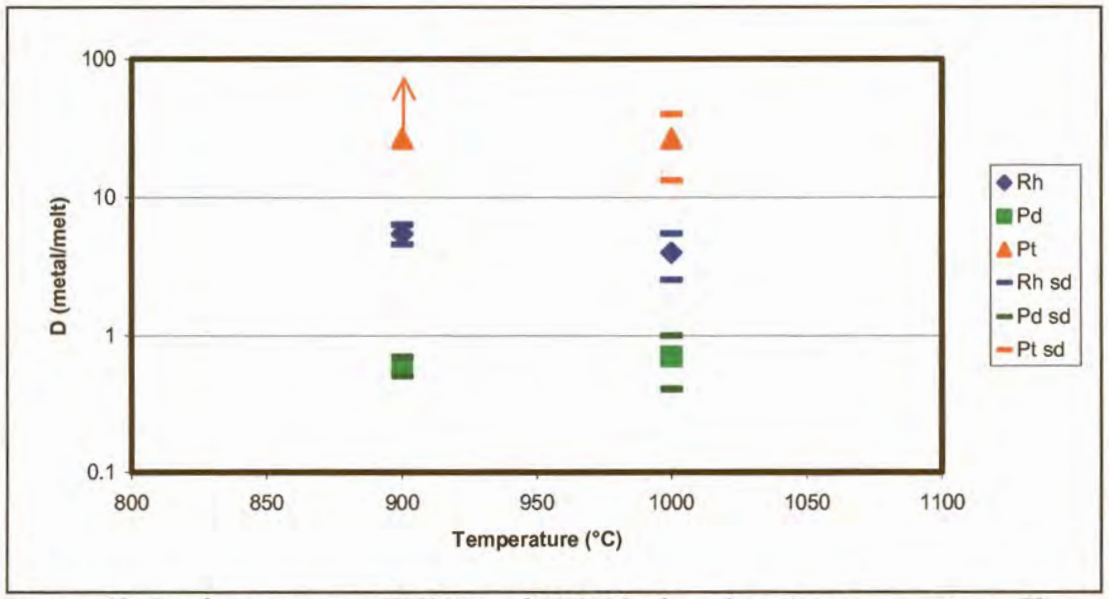


***Figure 48.*** *D of experiments HU381 and HU429 plotted against temperature. The trend of the Pd values is overshadowed by their associated errors. The 900°C Pt value is a minimum value (the arrow indicates possible higher values). Error bars show 3σ standard deviations.*

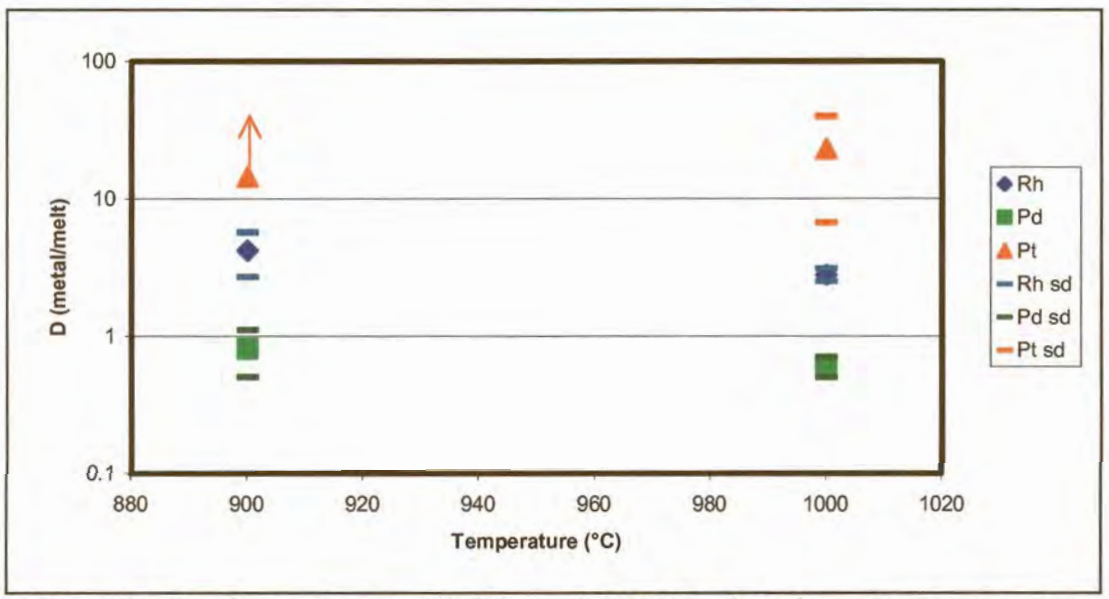


***Figure 49.*** *D of experiments HU393 and HU753 plotted against temperature. Both experiments contained 1000 ppm of each PGE. Error bars show 3σ standard deviations, and the arrow possible higher values. The trend displayed by $D_{Pt}$ is insignificant.*

The D for experiments HU393 and HU753 are plotted against temperature in Figure 49. Both experiments contained of 1000 ppm of each PGE. $D_{Rh}$ and $D_{Pd}$ decrease with increasing temperature. As the 900°C $D_{Pt}$ is a minimum value and the 1000°C $D_{Pt}$ has a very large associated error, no trend can be deduced.

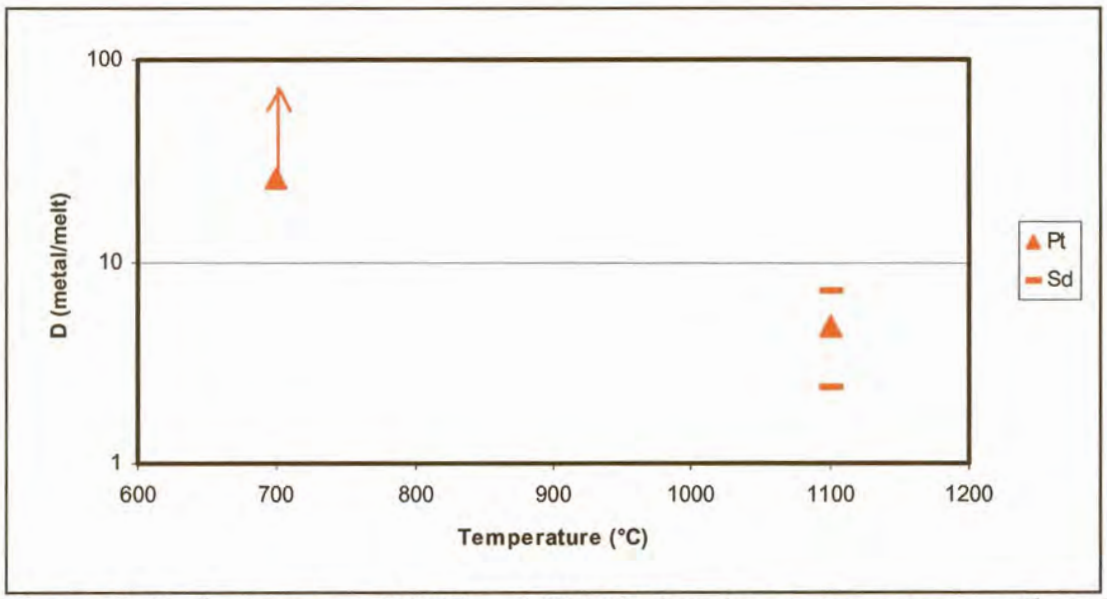


***Figure 50.*** *D of experiments HU731 and HU471 plotted against temperature. The value at 700°C is a minimum value (the arrow indicates possible higher values). Error bars show 3σ standard deviations.*

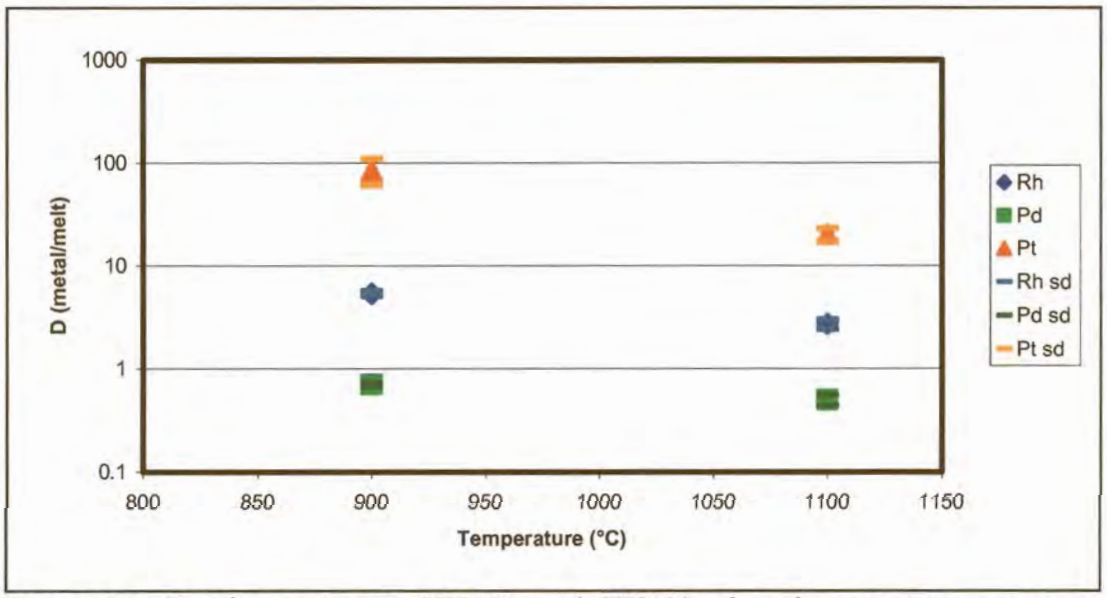


***Figure 51.*** *D of experiments HU441 and HU429 plotted against temperature. Both experiments contained 2000 ppm of each PGE. Error bars show 3σ standard deviations.*

Experiments HU731 and HU471 both contained 2000 ppm of only Pt in addition to Ni and S, and the D are compared in Figure 50. The 700°C partition coefficient is a minimum value, but still much larger than the 1100°C coefficient, including its error.

Figure 51 illustrates the dependency of D on temperature from the micro-PIXE data in Table 65, for experiments HU441 (1100°C) and HU429 (900°C). Both contained 2000 ppm of each PGE.

### 6.1.1.3. Variation of partition coefficients with PGE content

The PGE contents of the experiments apparently do not significantly influence the partition coefficients at these concentrations. Partition coefficients for experiments HU393 and HU381 determined by milli-PIXE (Table 64) are plotted in Figure 52. Both experiments were reacted at 1000°C, but HU393 contained 1000 ppm of each PGE while HU381 contained 2000 ppm of each PGE. The D's for the two experiments are very similar. Figure 53 shows the D of experiments HU753 (1000 ppm) and HU429 (2000 ppm), equilibrated at 900°C. The $D_{Pt}$ are both minimum values.

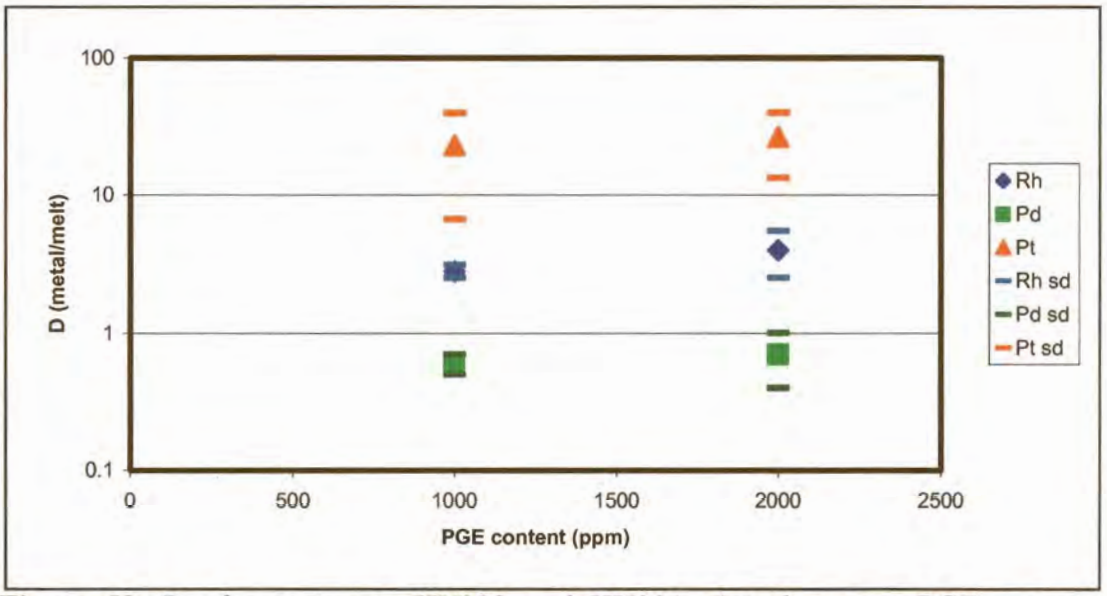


***Figure 52.*** *D of experiments HU393 and HU381 plotted against PGE content. Both experiments were equilibrated at 1000°C. Error bars show 3σ errors.*

The D calculated for experiments HU393, HU394, HU395 and HU412 from micro-PIXE data (Table 65) are plotted in Figure 54. Experiment HU393 contained 1000 ppm of each PGE, HU394 contained 6000 ppm of each PGE, and HU395 and HU412 each contained 10000 ppm of each PGE. At these concentrations, PGE content does not influence the partition coefficients.

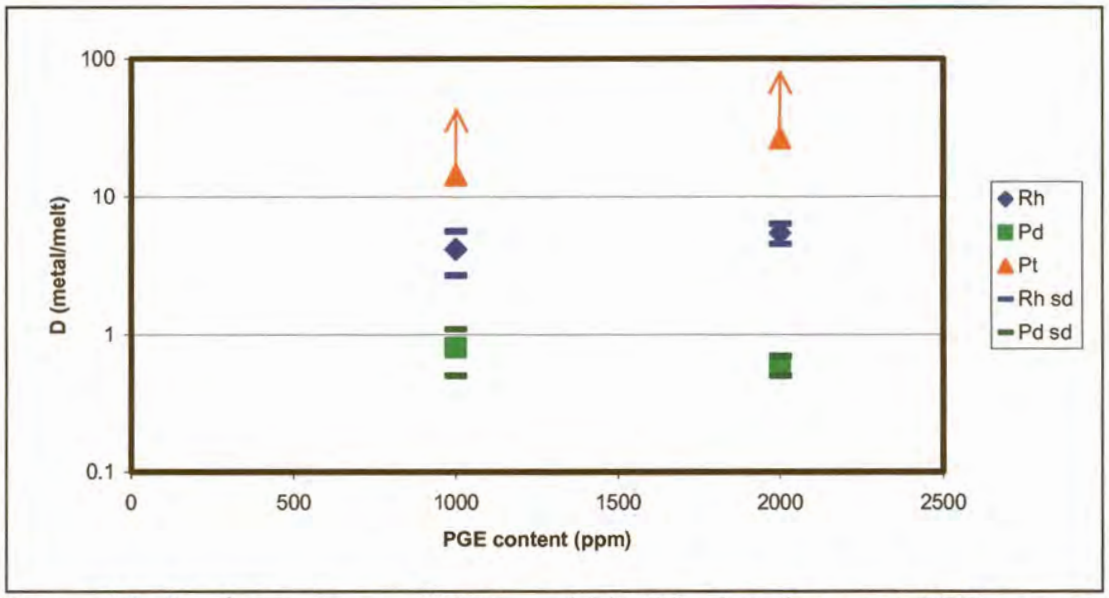


***Figure 53.*** *D of experiments HU753 and HU429 plotted against PGE content. Both experiments were equilibrated at 900°C. Error bars show 3σ standard deviations. The arrows indicate possible higher D values.*

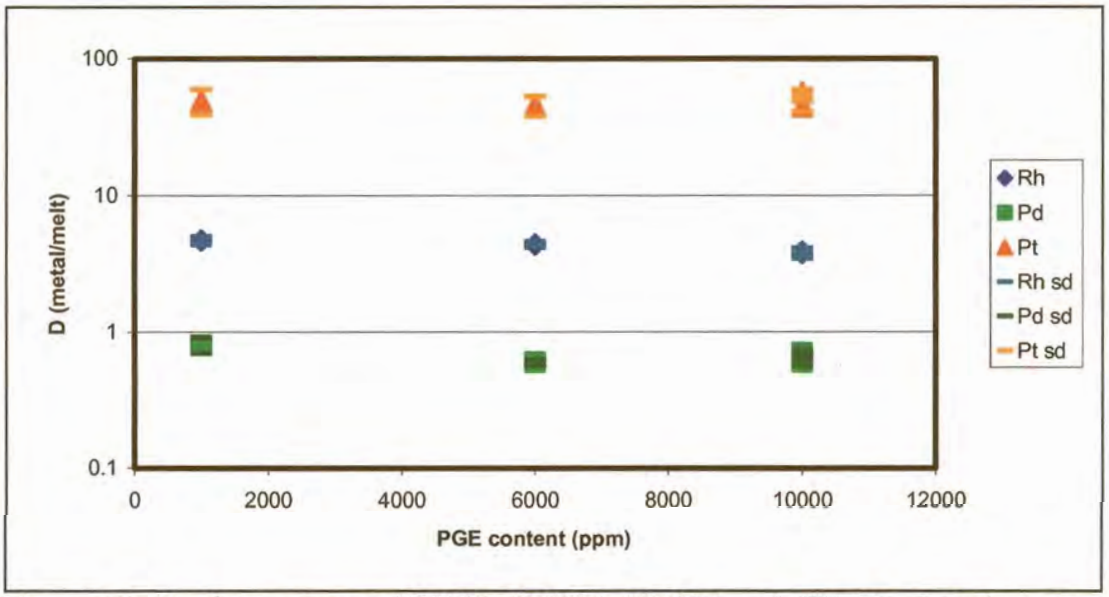


***Figure 54.*** *D of experiments HU393, HU394, HU395 and HU412 plotted against PGE content. All these experiments were equilibrated at 1000°C. Error bars show 3σ standard deviations.*

#### 6.1.1.4. Variation of partition coefficients resulting from the effect of PGE on each other

The influence of PGE on each other during partitioning is not unambiguous. According to the micro-PIXE analyses, partition coefficients appear to increase slightly when a PGE is in isolation from the other PGE, especially for Pd (compare values from experiments HU426, HU427, HU428 and HU429 – Table 65). The milli-PIXE $D_{Pd}$ (Table 64) for experiments HU427 and HU429 also suggests stronger differentiation of Pd into metal in the absence of other PGE (D value closer to 1). It seems that in the absence of other PGE the partitioning behaviour of the remaining PGE is amplified, but D drops when there is competition from other PGE.

#### 6.1.1.5. In conclusion

Pt, and to a lesser extent Rh, partition into the nickel, while Pd prefers to remain in the sulphide melt. Partition coefficients determined by different PIXE instruments vary, but remain in the same order of magnitude. The influence of equilibration temperature is most prominent with Pt and least with Pd. The amount of PGE in the experiments did not influence the partition coefficients, but the PGE partitioned more strongly into the preferred phase in the absence of other PGE.

## 6.2. The Cu-S system

### 6.2.1. Cu-rich melt - S-rich melt assemblage (1200°C)

Nernst partition coefficient: D = (PGE content in Cu-rich melt) / (PGE content in S-rich melt).

D were calculated from the milli-PIXE analyses discussed in section 5.2.1.2. (Table 31). The ratios and confidence intervals were obtained with resampling statistics (as discussed in

section 4.3.). Table 67 contains the D calculated from milli-PIXE results. Influence of initial bulk PGE contents, and presence or absence of other PGE in the systems, were investigated.

***Table 67.*** *D(Cu-rich melt/S-rich melt) for the PGE determined for the Cu-rich melt and S-rich melt from milli-PIXE results in Table 31.*

| Exp | Temp (°C) | PGE (ppm) | $D_{Rh}$ (± 1σ) | $D_{Pd}$ (± 1σ) | $D_{Pt}$ (± 1σ) |
|---|---|---|---|---|---|
| **HU442** | 1200 | 1000 | >9.2 | ~14 (~100) | >6.0 |
| **HU443** | 1200 | 2000 | | | >11.1 |
| **HU444** | 1200 | 2000 | | 7.5 (1.0) | |
| **HU445** | 1200 | 2000 | >34.9 | | |
| **HU450** | 1200 | 2000 | >21.4 | >6.3 | >3.3 |

### 6.2.1.1.Variation of partition coefficients with PGE content

Both experiments HU442 and HU450 contained all three PGE, but HU442 contained 1000 ppm of each PGE while HU450 contained 2000 ppm of each PGE. Five of the six coefficients are, however, minimum coefficients, and the associated error determined for the remaining $D_{Pd}$ with resampling statistics is extremely large, due to the large standard deviation of 0.01 wt% for Pd in S-rich melt.. The coefficients are plotted in Figure 55. No trends can be determined from this data set.

### 6.2.1.2. Variation of partition coefficients resulting from the effect of PGE on each other

Experiment HU450 contained 2000 ppm of each PGE, and experiments HU443, HU444 and HU445 each contained 2000 ppm of one PGE only (Table 67). Five of the six values are minimum values, and no deductions can be made.

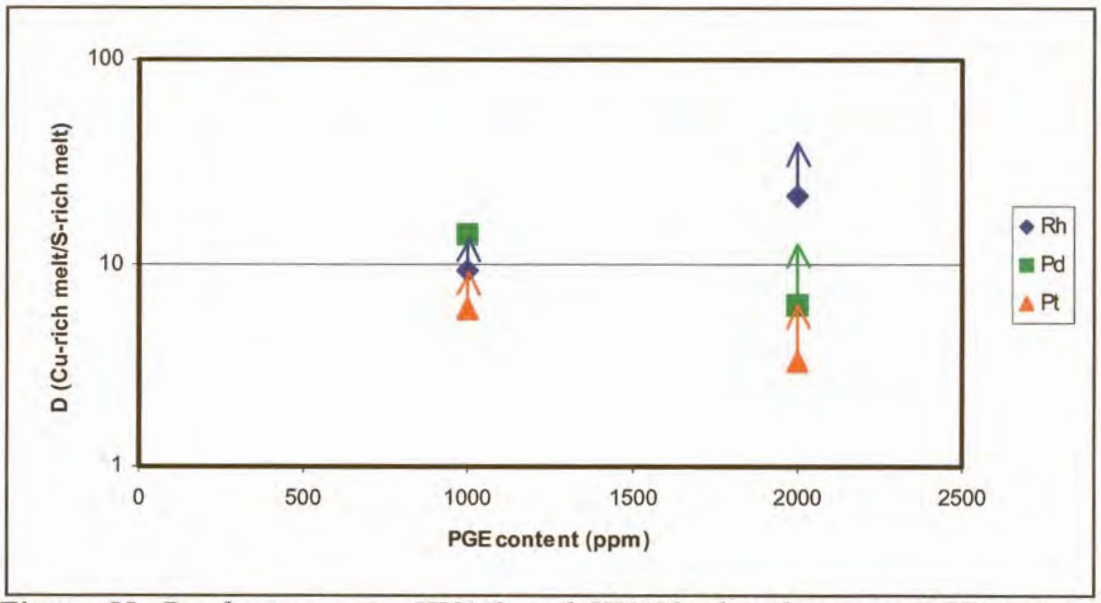


***Figure 55.*** *D of experiments HU442 and HU450 plotted against PGE content. Both experiments were equilibrated at 1200°C. Five of the six values are minimum values, as shown by the arrows, and the error of the remaining D value is too large to plot.*

#### 6.2.1.3.In conclusion

All three PGE strongly prefer the Cu-rich melt phase to the S-rich melt phase, with the consequence that precise PGE concentrations in the latter phase could not be determined. Only minimum detection limits could be obtained for most of the analyses of the S-rich melt. As a result, influence of PGE content and the effect of the absence and/or presence of other PGE, could not be determined.

### 6.2.2. Copper - digenite assemblage (1000°C and 800°C)

Nernst partition coefficient: D = (PGE content in metal) / (PGE content in digenite).

D were calculated from milli-PIXE analyses (Table 38) and micro-PIXE analyses (Table 41) discussed in section 5.2.2.2. The partition coefficients and confidence intervals were obtained with resampling statistics (as discussed in section 4.3.). Table 68 contains the D calculated from milli-PIXE results and Table 69 the D calculated from micro-PIXE results.

The effect of different PIXE instruments, the influence of PGE contents, and the presence or absence of other PGE in the experiments, were investigated.

***Table 68.*** *D(copper/digenite) for the PGE determined for copper and digenite from milli-PIXE results in Table 38. Values in italics are statistically unreliable.*

| Exp | Temp (°C) | PGE (ppm) | $D_{Rh}$ (± 1σ) | $D_{Pd}$ (± 1σ) | $D_{Pt}$ (± 1σ) |
|---|---|---|---|---|---|
| **HU382** | 1000 | 4000 | | | >15.0 |
| **HU384** | 1000 | 3000 | >58.7 | | |
| **HU385** | 1000 | 2000 | >23.9 | >29.2 | >13.5 |
| **HU387** | 1000 | 1000 | >15.0 | 23 (4.8) | *>1.2* |
| **HU465** | 1000 | 10000 | >167.5 | 100 (8) | >55.6 |
| **HU482** | 800 | 1000 | 45 (6) | >43.4 | >21.6 |

***Table 69.*** *D(copper/digenite) for the PGE determined for copper and digenite from micro-PIXE results in Table 41.*

| Exp | Temp (°C) | PGE (ppm) | $D_{Rh}$ (± 1σ) | $D_{Pd}$ (± 1σ) | $D_{Pt}$ (± 1σ) |
|---|---|---|---|---|---|
| **HU385** | 1000 | 2000 | >588.3 | 675 (80) | # |

# = standard deviations for analyses are too large to allow for reliable resampling

### 6.2.2.1.Variation of partition coefficients with different instruments

$D_{Pd}$ for experiment HU385 in both Tables 68 and 69 is the largest partition coefficient of the three PGE, followed by $D_{Rh}$, with $D_{Pt}$ being the lowest. As most of these values are minimum values, it is not possible to quantify real differences between the two data sets.

### 6.2.2.2.Variation of partition coefficients with equilibration temperature

Experiment HU387 was equilibrated at 1000°C and experiment HU482 at 800°C, but both contained 1000 ppm of each PGE. The PGE were difficult to detect in the digenite, therefore three of the values are minimum values. There is a decrease in the $D_{Pd}$ and $D_{Rh}$ from 800°C to 1000°C (Figure 56).

### 6.2.2.3.Variation of partition coefficients with PGE content

Experiments HU385, HU387 and HU465 were all equilibrated at 1000°C. HU387 contained 1000 ppm of each PGE, HU385 contained 2000 ppm of each PGE and HU465 contained 10000 ppm of each PGE. D appears to increase with increasing PGE content (Figure 57), but because so many of the values are minimum values, the trend is not conclusive.

### 6.2.2.4.Variation of partition coefficients resulting from the effect of PGE on each other

The influence of the PGE on each other during partitioning can be seen in experiments HU382, HU384 and HU385, all of which were equilibrated at 1000°C. $D_{Rh}$ and $D_{Pt}$ are minimum values, but Pt and Rh appear to partition more strongly into the metal in the absence of other PGE.

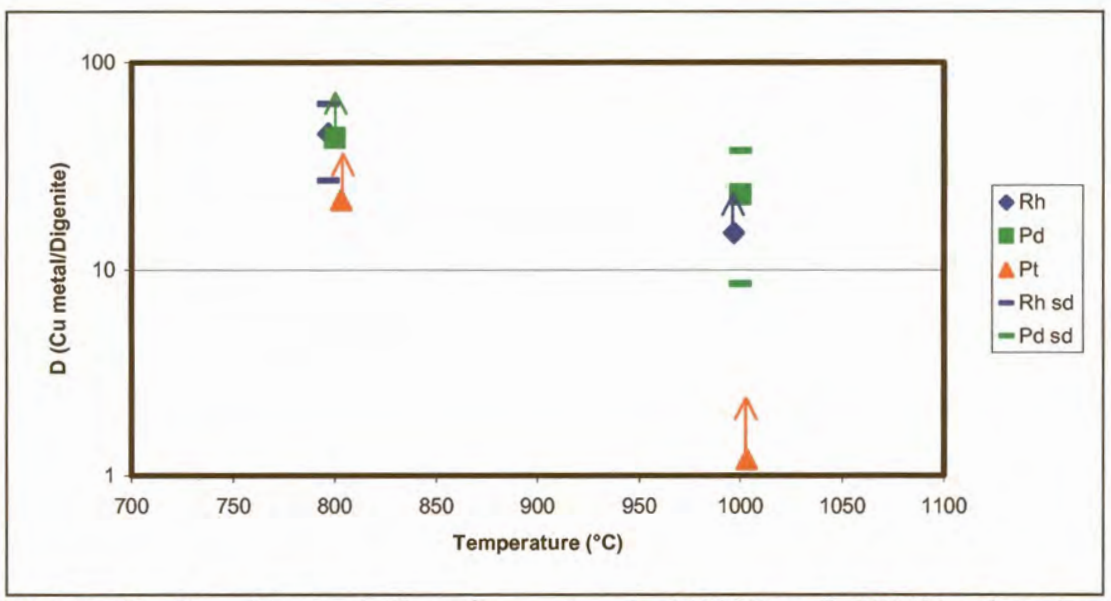


***Figure 56.*** *$D_{Rh}$, $D_{Pd}$ and $D_{Pt}$ of experiments HU387 and HU482 plotted against equilibration temperature. Both experiments contained 1000 ppm of each PGE. Four of the six values are minimum values, as shown by the arrows. Error bars show $3\sigma$ standard deviations.*

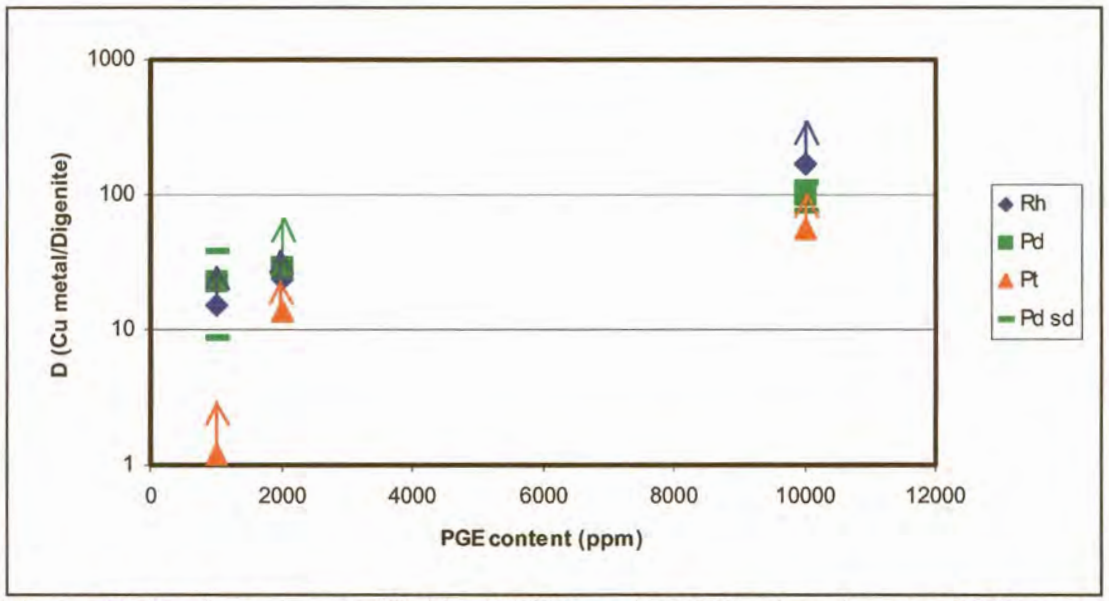


***Figure 57.*** *D of experiments HU385, HU387 and HU465, plotted against PGE content. All were equilibrated at 1000°C. Arrows indicate possible higher values for D, and error bars 3σ standard deviations.*

### 6.2.2.5.In conclusion

All PGE strongly prefer the copper to the digenite. Because most of the partition coefficients are minimum values, the trends can only be surmised. There are no definite differences between results from the two PIXE instruments, and it is uncertain whether PGE content, and the presence of other PGE, play a role during PGE partitioning. Temperature does influence the coefficients – they decrease with increasing temperature.

## 6.2.3. Digenite - melt assemblage (1000°C)

Nernst partition coefficient: D = (PGE content in melt) / (PGE content in digenite).

D were calculated from micro-PIXE analyses (Table 45) discussed in section 5.2.3.2. The partition coefficients and confidence intervals were obtained with resampling statistics (as discussed in section 4.3.). Table 70 presents the D's calculated from micro-PIXE results. The influence of PGE contents and presence or absence of other PGE in the experiments, were investigated.

***Table 70.*** *D(melt/digenite) for the PGE determined for the melt and digenite from micro-PIXE results in Table 45.*

| Exp | Temp (°C) | PGE (ppm) | $D_{Rh}$ (± 1σ) | $D_{Pd}$ (± 1σ) | $D_{Pt}$ (± 1σ) |
|---|---|---|---|---|---|
| **HU397** | 1000 | ?6000 | 3.8 (2.0) | 4.8 (0.4) | 17.4 (2.4) |
| **HU398** | 1000 | 10000 | 6.1 0.5 () | 4.0 (0.1) | 12.7 (1.0) |
| **HU411** | 1000 | 2000 | 43.1 (0.9) | 4.0 (0.1) | 23.6 (1.5) |
| **HU413** | 1000 | 1000 | 62.8 (3.1) | 2.9 (0.1) | 14.5 (2.2) |
| **HU418** | 1000 | 3000 | | | 12.7 (0.6) |
| **HU420** | 1000 | 2000 | 9.8 (0.4) | | |

? – A very PGE-rich drop separated from this experiment – discussed in 5.2.3.1 – remaining PGE content uncertain.

### 6.2.3.1. Variation of partition coefficients resulting from the effect of PGE on each other

Experiment HU411 contained 2000 ppm of each PGE, while experiment HU418 contained 3000 ppm Pt and HU420 2000 ppm Rh. The partition coefficients for the experiments that contain one PGE in isolation are lower than those where the PGE were combined.

### 6.2.3.2. Variation of partition coefficients with PGE content

The effect of PGE content on the partition coefficient is unclear in this case. When the D are plotted against the PGE contents (experiments HU398, HU411, HU413), there is a clear negative trend for Rh, and a suggestion of a negative trend for Pt. Pd remains constant (Figure 58).

### 6.2.3.3. In conclusion

All three PGE prefer the sulphide melt as opposed to the digenite, and Rh and Pt more so than Pd. $D_{Rh}$ and $D_{Pt}$ are higher when accompanied by other PGE than when in isolation. Higher PGE content correlates with a decrease in $D_{Rh}$.

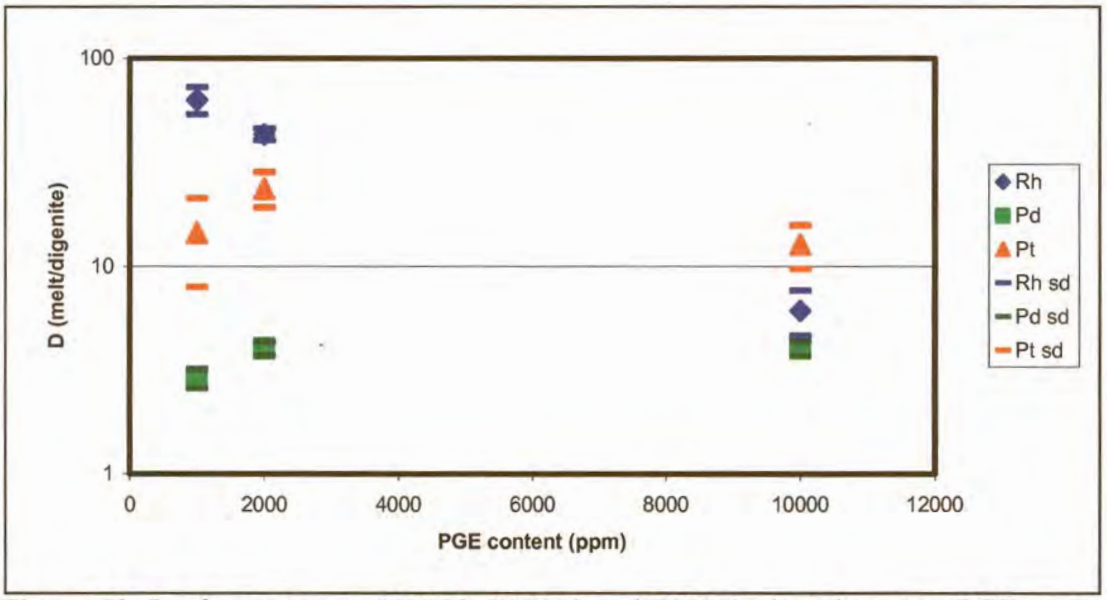


***Figure 58.*** *D of experiments HU398, HU411 and HU413 plotted against PGE content. All were reacted at 1000°C. Error bars show 3σ standard deviations.*

## 6.3. The Fe-S system

### 6.3.1. Iron – Fe-S melt assemblage (1200°C to 1000°C)

Nernst partition coefficient: D = (PGE content in metal) / (PGE content in melt).

D were calculated from milli-PIXE analyses (Table 55), discussed in section 5.3.1.2. The partition coefficients and confidence intervals were obtained with resampling statistics (as discussed in section 4.3.). Table 71 contains the D calculated from milli-PIXE results. The standard deviations of these partition coefficients are very large, and it is very difficult to observe any trends or to compare different coefficients. Rh and Pt show a preference for the iron. $D_{Pd}$ changes from slightly incompatible at higher temperatures to slightly compatible to iron at lower temperatures.

The presence of oxygen in these experiments makes it possible to determine the exact $fO_2$ and $fS_2$ conditions under which the experiments were reacted, as O, S and Fe were all present and equilibrated. Phase stability diagrams from HSC software were consulted, and log $pO_2$ - log $pS_2$ coordinates of the Fe-FeO-FeS triple points at 1200°C, 1100°C and

1000°C transformed to $fO_2$- $fS_2$ coordinates. At 1200°C an $fO_2$ of 2.79 x $10^{-13}$ and a $fS_2$ of 1.63 x $10^{-5}$ would have prevailed, at 1100°C an $fO_2$ of 1.13 x $10^{-14}$ and a $fS_2$ of 2.71 x $10^{-6}$, and at 1000°C an $fO_2$ of 2.73 x $10^{-16}$ and a $fS_2$ of 3.21x$10^{-7}$. At lower temperatures smaller amounts of oxygen are required to form oxides with Fe, which explains why the 1000°C experiments contain the most oxides.

***Table 71.*** *D(iron/melt) for the PGE determined from milli-PIXE results in Table 55.*

| Exp | Temp (°C) | PGE (ppm) | $D_{Rh}$ (± 1σ) | $D_{Pd}$ (± 1σ) | $D_{Pt}$ (± 1σ) |
|---|---|---|---|---|---|
| **HU825** | 1200 | 2200 | | | *214.0 (#)* |
| **HU826** | 1200 | 2600 | | *0.98(0.69)* | |
| **HU827** | 1200 | 2000 | *4.27(#)* | | |
| **HU734** | 1100 | 2400 | | | - |
| **HU735** | 1100 | 2400 | | *0.8(~4.0)* | |
| **HU736** | 1100 | 2000 | *1.2(#)* | | |
| **HU843** | 1000 | 2200 | | *1.92(#)* | |
| **HU844** | 1000 | 2000 | >2.0 | | |
| **HU845** | 1000 | 2000 | >2.1 | >1.2 | - |
| **HU849** | 1000 | 6000 | >2.2 | - | >1.1 |
| **HU850** | 1000 | 10000 | *8(#)* | *1.8* | *1.6* |

# = standard deviations for analyses are too large to allow for reliable resampling

### 6.3.2. Pyrrhotite – sulphide melt assemblage (1100°C)

Nernst partition coefficient: D = (PGE content in melt) / (PGE content in pyrrhotite).

D were calculated from milli-PIXE analyses (Table 59) discussed in section 5.3.2.2. The partition coefficients were obtained with resampling statistics (as discussed in section 4.3.). Table 72 contains the D calculated from milli-PIXE results. Minimum partition coefficients were determined for Rh, Pd and Pt. All PGE prefer the sulphide melt.

***Table 72.*** *D(melt/pyrrhotite) for the PGE determined from milli-PIXE results in Table 59.*

| Exp | Temp (°C) | PGE (ppm) | $D_{Rh}$ (± 1σ) | $D_{Pd}$ (± 1σ) | $D_{Pt}$ (± 1σ) |
|---|---|---|---|---|---|
| **HU737** | 1100 | 2000 | | | >3.8 |
| **HU738** | 1100 | 2000 | | >10.5 | |
| **HU739** | 1100 | 2000 | >3.7 | | |

### 6.3.3. Iron - troilite assemblage (900°C)

Nernst partition coefficient: D = (PGE content in metal) / (PGE content in troilite).

D were calculated from milli-PIXE analyses (Table 63) discussed in section 5.3.3.2. The partition coefficients and confidence intervals were obtained with resampling statistics (as discussed in section 4.3.). Table 73 contains the D calculated from milli-PIXE results. All PGE favour the metal as opposed to troilite.

***Table 73.*** *D(iron/troilite) for the PGE determined from milli-PIXE results in Table 63.*

| Exp | Temp (°C) | PGE (ppm) | $D_{Rh}$ (± 1σ) | $D_{Pd}$ (± 1σ) | $D_{Pt}$ (± 1σ) |
|---|---|---|---|---|---|
| **HU434** | 900 | 1800 | | | >2.8 |
| **HU435** | 900 | 2600 | | - | |
| **HU436** | 900 | 2200 | *>2.1* | | |
| **HU756** | 900 | 1000 | >3.5 | *1.2(0.7)* | >1.6 |

## 6.4. Mass balance calculations

Mass balances were calculated by using the EPMA analyses of co-existing phases, the PGE content in both phases as determined by PIXE, starting compositions, and the lever-rule. Mass balances were calculated for experiments in which:

- PGE contents in both co-existing phases were above the detection limit.
- Major element compositions of both phases in the experiment could be determined accurately in terms of the two major elements concerned (i.e. no accidental contamination).

The mass balance errors - expressed as percentages in relation to the initial amount of PGE weighed into the experiments - for experiments of the Ni-S system are shown in Tables 74 and 75. The Ni-S system was selected for testing and interpreting sources of error, as it contained the largest number of analysed experiments of a single assemblage. The mass balances indicate that surplus PGE were detected in almost all of the experiments, with few exceptions.

***Table 74.*** *Mass balance errors calculated from micro-PIXE analyses of PGE contents of the Ni-S system, expressed as percentages of the original PGE content.*

| Exp | Temp (°C) | Rh - % error | Pd - % error | Pt - % error |
|---|---|---|---|---|
| HU441 | 1100 | 9.64 | 16.71* | 29.00 |
| HU437 | 1100 | - | 32.33* | - |
| HU393 | 1000 | 42.40 | 38.33* | 75.10 |
| HU394 | 1000 | 40.39 | 5.59 | 95.50 |
| HU395 | 1000 | 40.93 | 60.16 | 64.75 |
| HU412 | 1000 | 20.80 | 1.36 | 25.75 |
| HU429 | 900 | 27.71 | 1.92 | 35.34 |
| HU426 | 900 | - | - | 51.90* |
| HU427 | 900 | - | 0.51* | - |
| HU428 | 900 | 11.07* | - | - |

* - Element under-represented by PIXE measurements.

***Table 75.*** *Mass balance errors calculated from milli-PIXE analyses of PGE contents of the Ni-S system, expressed as percentages of the original PGE content.*

| Exp | Temp (°C) | Rh - % error | Pd - % error | Pt - % error |
|---|---|---|---|---|
| HU733 | 1100 | 100.42 | 46.06 | 3.51* |
| HU731 | 1100 | - | - | 33.34* |
| HU393 | 1000 | 102.50 | 27.72 | 41.25 |
| HU381 | 1000 | 93.67 | 88.36 | 86.65 |
| HU753 | 900 | 56.31 | 6.58* | - |
| HU429 | 900 | 53.23 | 54.13 | - |
| HU427 | 900 | - | 69.14 | - |
| HU469 | 700 | 71.07 | 3.12 | - |
| HU473 | 700 | 31.33 | - | - |

* - Element under-represented by PIXE measurements.

Overall the mass balance errors are very large, averaging more than 50% for the milli-PIXE data and more than 30% for the micro-PIXE data. To evaluate whether the mass balance errors are dependent on analytical uncertainty, the relationship between the mass balance percentage errors and the partition coefficient standard deviations as percentage errors of the partition coefficients was evaluated. The standard deviations of the partition coefficients were determined from the analytical errors of the PIXE data, and are therefore known to be solely dependent on analytical error. Figure 59 shows this relationship for the micro-PIXE data, and Figure 60 for the milli-PIXE data.

The positive correlation between analytical error and mass balance percentage error for the micro-PIXE data (Figure 59) indicates that the mass calibration error is reflected in the errors of the partition coefficients for this data. It is therefore implied that the mass balance errors are mainly dependent on analytical error, and not experimental error.

However, there is no positive correlation between percentage analytical error and percentage error from mass balance calibration for the milli-PIXE data (Figure 60). As errors other than analytical error have been eliminated by the positive relationship for the

micro-PIXE data (Figure 59), and errors are implied to be mainly analytical, it is clear that the analytical error in the milli-PIXE data is more random and unpredictable.

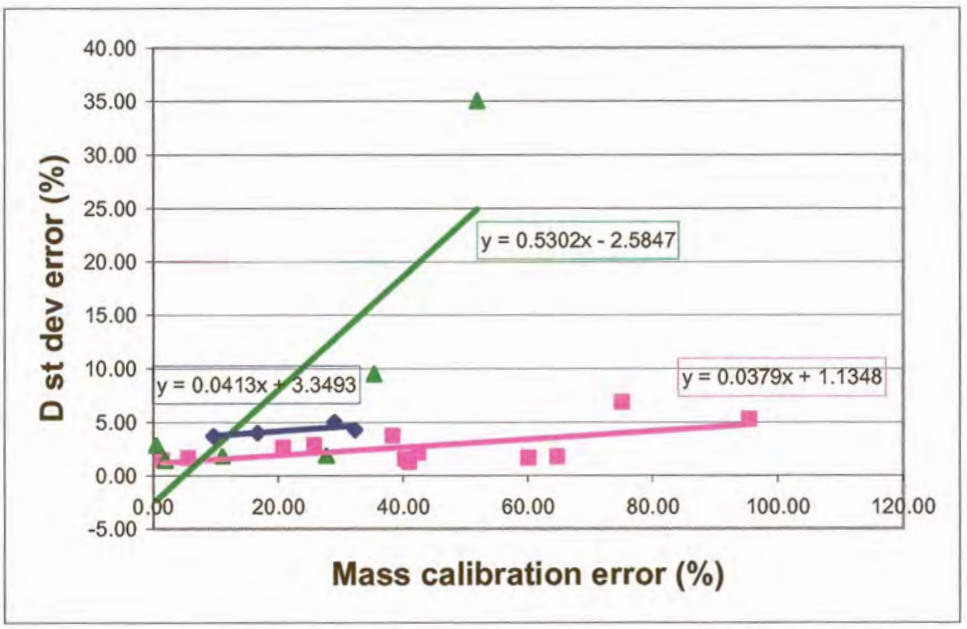


***Figure 59.*** *The linear relationship between mass calibration errors and standard deviation errors for micro-PIXE data at 1100°C (●), 1000°C (■) and 900°C (▲) are indicated by the regression lines. The R value for the 1100°C data is 0.77, for the 1000°C data 0.60, and for the 900°C data 0.82.*

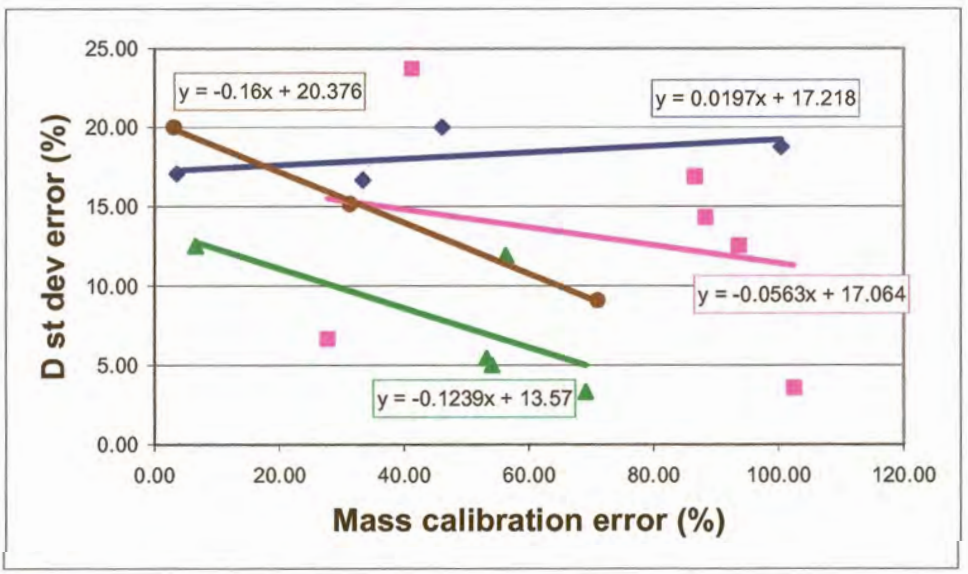


***Figure 60.*** *The linear relationship between mass calibration errors and standard deviation errors for milli-PIXE data at 1100°C (●), 1000°C (■), 900°C(▲) and 700°C (●) are indicated by the regression lines. The R value for the 1100°C data is 0.52, for the 1000°C data 0.24, for the 900°C data 0.70, and for the 700°C data 1.00.*

In hindsight, analytical errors on both instruments could have been checked more thoroughly, for example by the compilation of correlation curves for one or more sets of standards with increasing contents of an element, or the analysis of standards with known trace contents. However, as PIXE is frequently portrayed to be standard independent (Ryan *et al.*, 1990), further evaluation of this problem was not considered a necessity at the time of analysis. Development of the milli-PIXE line at the AEC for the analysis of matrixes as investigated in this study is ongoing, but resolving fundamental problems of PIXE analysis, as encountered in this study, goes way beyond the scope of this project. The instrument is presently not accessible for analytical work, and the root of the problem cannot be evaluated at present. However, future measurements aimed at resolving these problems will include preparation of appropriate standards, as well as re-evaluation of the collected spectra and a refinement of the partition coefficients.

The mass balance errors should reflect all possible introduced errors, such as weighing errors, sample separation during equilibration, and analytical error, but the latter is believed to predominate.

# 7. Conclusions

## 7.1. The Ni-S system

The partition coefficients of Rh, Pd and Pt between metallic nickel and sulphide melt were discussed in Section 6.1.1. and are presented in Tables 64 and 65.

- Pt and Rh are compatible with nickel (partition coefficients > 1), while Pd is incompatible. Partition coefficients vary from 2 to 10 for Rh, from 0.5 to 0.9 for Pd and from 4 to 220 for Pt. These results compare favourably with the investigation by Urban *et al.* (1995), who reported Pt to prefer alloys with Ni and PGE, and Pd to favour the sulphides. Rh, however, was reported also to prefer PGE sulphides, whereas it prefers the nickel in this investigation. This is probably because the PGE content in the melt in the present investigation is too low to form PGE sulphides. Fleet and Stone (1991) also reported enrichment of Pt in alloy in the Fe-Ni-S system, and relative enrichment of Pd in sulphide liquid as opposed to alloy. They found Pd partitioning into Fe alloy, but in the absence of Fe in the alloys it favoured the sulphide. As their partition coefficients were determined between iron and sulphide liquid, they cannot be compared to the coefficients determined for the Ni-S system. Fleet *et al.* (1999) reported partition coefficients in the Fe-Ni-S system between solid metal and liquid metal sulphide of 40 – 300 for Pt and 0.7 – 1.47 for Pd, which compares favourably with this investigation. The absence of Fe in the alloy in these Ni-S experiments probably influences Pd to partition into the melt, so that the coefficients remain smaller than 1.

- As shown in Tables 64 and 65, there are significant differences between the partition coefficients from the two different PIXE instruments. It is generally accepted that errors of PGE partition coefficients determined at low PGE contents are large. According to Barnes *et al.* (1997) errors on PGE partition coefficients are

in the order of 20 – 50%. Such errors could eliminate the difference between the two PIXE instruments in this investigation.

- The partition coefficients are temperature dependent – they decrease as the temperature increases. Fleet *et al.* (1999) stated that PGE partition coefficients in the Fe-Ni-S system are much less dependent on temperature than on the S content in the melt, and that with increasing S content in the melt the PGE become more siderophile. At lower temperatures the S content in the Ni-S melt in this investigation is higher than at high temperatures (see phase diagram in Figure 11). For the Ni-S system in this investigation it is not possible to determine whether it is the temperature or the S content in the melt that is responsible for the change of the partition coefficients.

- The partition coefficients are not significantly influenced by the PGE contents investigated in this study. This supports the statement by Barnes *et al.* (1997) that at low PGE contents the partition coefficients are independent of their concentration.

- The PGE partition significantly more strongly into metal in the absence of other PGE, especially Pd.

## 7.2. The Cu-S system

Partition coefficients for Rh, Pd and Pt between Cu-rich melt and S-rich melt were discussed in Section 6.2.1. and are presented in Table 67. Partition coefficients between copper and digenite were determined in Section 6.2.2. and are shown in Tables 68 and 69, and partition coefficients between digenite and melt were determined in Section 6.2.3. and are presented in Table 70.

- Rh, Pd and Pt all partition into the Cu-rich melt as opposed to the sulphide melt (partition coefficients > 1), but these coefficients are mostly minimum values, and the exact values are unknown. The partition coefficients determined in the present

investigation for Rh are generally larger than 10, for Pd about 7 and for Pt larger than 3. Gerlach *et al.* (1972) determined a coefficient of 2000 for Pt into Cu, Schlitt and Richards (1975) determined partition coefficients of 167 for Pd and 2500 for Pt into Cu. Taylor (1983) determined an experimental partition coefficient of 110 for Rh, and calculated coefficients of 11 for Rh, 25 for Pd and 6800 for Pt. Burylev *et al.* (1974) determined partition coefficients of 80 for Pd and 2000 for Pt. The Rh partition coefficients from this investigation compare favourably, while the Pd coefficients are a little low and the Pt coefficients should be very high.

- The partition coefficients between metal and digenite for this investigation are generally larger than 15 for Rh, larger than 20 for Pd and larger than 10 for Pt - all three PGE are compatible with the metal.

- Partition coefficients of between about 4 and 60 for Rh, between 3 and 5 for Pd and between 12 and 24 for Pt were determined between melt and digenite in this investigation - all PGE favouring the melt. Spectra were interpreted with the GEOPIXE software, and these coefficients could be questionable (see Section 6.1.1.1.).

- For the copper-digenite assemblage there is an indication that the partition coefficient increases as the bulk PGE content increases, but for the other two assemblages it is not possible to draw any conclusions.

## 7.3. The Fe-S(±O) system

Partition coefficients for PGE between iron and melt, pyrrhotite and melt and iron and troilite were discussed in Sections 6.3.1., 6.3.2. and 6.3.3., and the coefficients are presented in Tables 71, 72 and 73. The partition coefficients determined for this system are very unreliable, due to experimental difficulties and the presence of O in most of the experiments.

- Most of the partition coefficients determined for the metal-melt assemblage are statistically unreliable. The Rh coefficient is apparently larger than 2, favouring the metal, the Pd coefficient varies from slightly compatible to slightly incompatible in the metal, and the Pt coefficients are larger than 1, favouring the metal, but are very unreliable. Fleet and Stone (1991) reported alloy/sulphide liquid partition coefficients of 1 to 2 for Pd, 30 to 110 for Rh and > 1000 for Pt. Chabot and Drake (1997) determined a Pd partition coefficient of between 0.5 and 2 for metal / liquid. With increasing S content of the liquid the Pd became more compatible with the solid metal – as was also determined in this investigation. This finding supports the statements by Fleet *et al.* (1999) and Li *et al.* (1996) that PGE partitioning is dependent on the S content of the melt.

- In the melt-pyrrhotite assemblage the partition coefficients are all larger than 1 - all PGE are compatible with the melt. The Rh and Pt partition coefficients are larger than about 4, and the Pd partition coefficient larger than 10. Fleet and Stone (1991) found Rh the only PGE to be slightly compatible with the sulphide.

- In the metal-troilite assemblage all three PGE favour the metal - all partition coefficients are larger than 1. The Rh and Pt coefficients are larger than 2, and the Pd coefficient larger than 1. Jones *et al.* (1986) reported a metal/troilite partition coefficient of 150 for Pd.

- No assumptions on the influence of bulk PGE content, temperature or the influence of other PGE can be made, due to the unreliability of the partition coefficients.

## 7.4. PGE partitioning in general

In assemblages with alloy, such as copper – digenite, Cu-rich melt – sulphide melt, iron – sulphide melt, iron – troilite and nickel – sulphide melt, Pt and Rh are always concentrated in the alloy phases. In the nickel – sulphide melt assemblage, Pd is the only PGE that is not compatible in the metal, and is concentrated in the melt, and in the iron – sulphide melt

assemblage, Pd varies from slightly incompatible at higher temperatures to slightly compatible at lower temperatures in the metal. Pt partitioning into iron is surprisingly low, but can possibly be attributed to the presence of O. All PGE avoid the sulphide phases – digenite, pyrrhotite and troilite – and are being concentrated in the co-existing sulphide melt or alloy.